JCB Journal of Cell Biology

ARTICLE

Entosis and apical cell extrusion constitute a tumor-suppressive mechanism downstream of Matriptase

Joy Armistead[1,2], Julia Hatzold[1], Anna van Roye[1], Evelin Fahle[1], and Matthias Hammerschmidt[1,2,3]

The type II transmembrane serine protease Matriptase 1 (ST14) is commonly known as an oncogene, yet it also plays an understudied role in suppressing carcinogenesis. This double face is evident in the embryonic epidermis of zebrafish loss-of-function mutants in the cognate Matriptase inhibitor Hai1a (Spint1a). Mutant embryos display epidermal hyperplasia, but also apical cell extrusions, during which extruding outer keratinocytes carry out an entosis-like engulfment and entrainment of underlying basal cells, constituting a tumor-suppressive effect. These counteracting Matriptase effects depend on EGFR and the newly identified mediator phospholipase D (PLD), which promotes both mTORC1-dependent cell proliferation and sphingosine-1-phosphate (S1P)–dependent entosis and apical cell extrusion. Accordingly, hypomorphic *hai1a* mutants heal spontaneously, while otherwise lethal *hai1a* amorphs are efficiently rescued upon cotreatment with PLD inhibitors and S1P. Together, our data elucidate the mechanisms underlying the double face of Matriptase function in vivo and reveal the potential use of combinatorial carcinoma treatments when such double-face mechanisms are involved.

Introduction

Matriptase-1, also named ST14, is a type 2 transmembrane serine protease that is expressed in most epithelia to regulate their integrity (List et al., 2009). Its activity is tightly regulated by its coexpressed cognate transmembrane inhibitor Hai1, also named Spint1. Via its extracellular protease domain, Matriptase is capable of activating multiple pro-oncogenic signaling pathways, and levels of both Matriptase and Hai1 are dysregulated in many cancers of epithelial origin (Oberst et al., 2002).

Zebrafish at embryonic and larval stages have a bilayered epidermis composed of an outer layer of peridermal cells and an inner layer of basal keratinocytes, which are attached to a basement membrane that separates the epidermis from the underlying dermis. It is therefore a simple in vivo skin system, genetically tractable and easily modified by pharmaceuticals. Zebrafish mutants in the Matriptase inhibitor Hai1a display hyper-proliferation of basal keratinocytes at embryonic stages and disruption of epidermal architecture, including loss of basement membrane integrity. The relevant pathways activated by Matriptase are unclear, but, unlike in studied mammalian systems, they do not seem to involve HGF-cMet signaling (Carney et al., 2007; Lee et al., 2000). Interestingly, zebrafish *hai1a* mutants before hatching shed epidermal cells into the chorion (Carney et al., 2007), which led us to question whether this might contribute to the spontaneous healing of the mutants and might be a controlled process similar to apical cell extrusion. To date, apical cell extrusion, a tumor-suppressive process due to its ability to relieve cells from an over-crowded environment (Eisenhoffer et al., 2012; Marinari et al., 2012), or to remove transformed cells from an otherwise normal epithelium (Slattum et al., 2009), has been mainly studied in cell monolayers in vitro. In this context, cells to be extruded signal to their neighbors via the lipid second messenger sphingosine-1-phosphate (S1P), which is sensed by the G-protein–coupled receptor S1P receptor 2 (S1pr2; Gu et al., 2011). Activation of S1pr2 in surrounding cells activates a signaling cascade that culminates in the formation and contraction of an actin-myosin ring around the base of the extruding cell, squeezing it apically out of the epithelium without compromising epithelial integrity. In mice, overexpression of S1pr2 is sufficient to reduce the size and metastatic potential of orthotopic tumors (Gu et al., 2015). However, the exact contributions of cell extrusion to tumor suppression in vivo have not been examined in detail.

Using a chemical inhibitor screen, we uncovered a Matriptase–Par2b–EGFR–phospholipase D (PLD)–mTOR signaling

[1]Institute of Zoology, Developmental Biology Unit, University of Cologne, Cologne, Germany; [2]Center for Molecular Medicine Cologne, University of Cologne, Cologne, Germany; [3]Cologne Excellence Cluster on Cellular Stress Responses in Aging-Associated Diseases, University of Cologne, Cologne, Germany.

Correspondence to Matthias Hammerschmidt: mhammers@uni-koeln.de.

© 2019 Armistead et al. This article is distributed under the terms of an Attribution–Noncommercial–Share Alike–No Mirror Sites license for the first six months after the publication date (see http://www.rupress.org/terms/). After six months it is available under a Creative Commons License (Attribution–Noncommercial–Share Alike 4.0 International license, as described at https://creativecommons.org/licenses/by-nc-sa/4.0/).

Downloaded from http://rupress.org/jcb/article-pdf/219/2/e201905190/1622245/jcb_201905190.pdf by guest on 05 December 2025

axis responsible for both (oncogenic) hyperproliferation and (tumor-suppressive) cell extrusion in the bilayered epidermis of *hai1a* mutant embryos. We also identified an unexpected mechanism for the removal of preneopastic cells from the underlying basal layer, whereby outer peridermal cells engulf basal keratinocytes before their own extrusion. This engulfment displays characteristics of entosis, a nonapoptotic "cell-in-cell" death process with tumor-suppressive potential, which has been largely studied in vitro but not yet described in the context of apical cell extrusion (Krishna and Overholtzer, 2016; Overholtzer et al., 2007). Finally, we show that suppression of S1P signaling and thereby entosis and apical cell extrusion worsen the Matriptase-mediated preneoplastic phenotypes of *hai1a* mutants, while their promotion leads to rapid healing, together strong indicators that entosis and apical cell extrusion are indeed tumor suppressor mechanisms in this context.

Results

The skin phenotype of zebrafish *hai1a*^{hi2217} mutants heals spontaneously

We and others previously described the *hai1a*^{hi2217} zebrafish skin mutant, which contains a viral insertion upstream of the first coding exon of the Matriptase inhibitor *hai1a*, leading to reduced transcript levels (Carney et al., 2007; Mathias et al., 2007). During the first days of development, basal keratinocytes in the epidermis of homozygous mutant embryos exhibit increased motility and proliferation. In addition, innate immune cells infiltrate the epidermis, and transcript levels of the matrix metalloprotease gene *mmp9* are significantly up-regulated, accompanied by compromised basement membrane integrity (Carney et al., 2007; LeBert et al., 2015; Mathias et al., 2007; Schepis et al., 2018; Fig. 1 I). These defects are all rescued by *matriptase1a* (*mat1a*) knockdown (Carney et al., 2007; Mathias et al., 2007), indicating that increased Matriptase activity underlies the phenotype. Interestingly, these skin defects of *hai1a*^{hi2217} mutants heal spontaneously to a large extent by the fourth day of development (Fig. 1, A–B′), including a normalization of epidermal BrdU incorporation rates between 48 and 96 h postfertilization (hpf; Fig. 1 F, F′, and H′). Indeed, *hai1a*^{hi2217} homozygotes are viable (Fig. 1 N) and fertile as adults.

In the course of an N-ethyl-N-nitrosourea mutagenesis screen for skin mutants (Carney et al., 2010), we recovered another *hai1a* allele, *fr26* (hereafter *hai1a*^{fr26}), which contains a nonsense c.C445T; p.Q149X mutation in exon 3 (Fig. 1, J and K), leading to a C-terminal truncation of the protein lacking the Kunitz-like domains that inhibit Matriptase, as well as the transmembrane domain (Fig. 1 L). Furthermore, quantitative RT-PCR of 48-hpf cDNA revealed a reduction of *hai1a* transcript levels down to 17% of sibling values, most likely due to nonsense-mediated decay (Fig. 1 M). Together, this suggests that in contrast to *hai1a*^{hi2217}, which is hypomorphic, the novel *hai1a*^{fr26} allele likely represents a functional null/amorph.

Consistently, *hai1a*^{fr26} mutants exhibit a similar, but generally stronger, embryonic skin phenotype (Fig. 1, A–C′), including higher proliferation rates (Fig. 1, E–H) and *mmp9* transcript levels (Fig. 1 I), but also a slight developmental delay (Fig. S1, A and B), and more pronounced skin inflammation (Fig. S1 C). As in *hai1a*^{hi2217} mutants (Carney et al., 2007), epidermal defects are independent of skin inflammation, as all investigated phenotypic traits persisted even after suppression of the myeloid cell lineage by *pu.1* morpholino oligonucleotide (MO) injection (Rhodes et al., 2005; Fig. S1, C–H). However, in contrast to *hai1a*^{hi2217} mutants, *hai1a*^{fr26} mutants do not recover (see below), with even further increased epidermal proliferation rates at 96 hpf compared with 48 hpf (Fig. 1, G, G′, and H), and death of mutants between 4 and 8 d postfertilization (dpf; Fig. 1 N).

Loss of Matriptase inhibition activates a Par2b-EGFR-PLD-mTORC1 signaling cascade

To gain better insights into the relevant molecular pathways downstream of Matriptase in *hai1a*^{hi2217} hypomorphs, we screened two chemical libraries (Biomol ICCB known bioactives, Enzo Life Sciences, 472 compounds; Food and Drug Administration–approved drugs, Enzo Life Sciences, 640 compounds; Wiley et al., 2017) for small compounds alleviating or enhancing mutant epidermal morphology between 24 and 96 hpf. In addition, mutants were treated with compounds not included in these libraries, but formerly reported to normalize skin morphology in other zebrafish mutants (Carney et al., 2007; Hatzold et al., 2016; Mathias et al., 2007; Reischauer et al., 2009). Several compounds led to a striking phenotypic alleviation, including two whose substrates had been described previously in the context of Matriptase: the ErbB2/EGFR inhibitor PD168393 and the mTORC1 inhibitor rapamycin.

Rapamycin has been shown to rescue epithelial carcinogenesis in a mouse model of up-regulated Matriptase signaling (Szabo et al., 2011), while EGFR, which upon increased activity can also be oncogenic (Zandi et al., 2007), can be constitutively activated either by Matriptase itself (via proteolytic cleavage in the EGFR ectodomain; Chen et al., 2008) or by the Matriptase substrate Par2, a G-protein–coupled receptor (via transactivation of EGFR; Ye et al., 2014). Consistently, injection of zebrafish *hai1a*^{hi2217} mutants with a *par2b* MO or treatment of mutant embryos with PD168393 alleviated the morphological symptoms (Fig. 2, C, D, and G), attenuated proliferation rates in the skin (Fig. 2, C′′, D′′, and J), and rescued *mmp9* levels (see Fig. 5), in agreement with recent data obtained by others (Schepis et al., 2018). A very similar rescue was obtained upon treatment of mutant embryos with the mTORC1 inhibitor rapamycin (Fig. 2, F, F′′, G, and J). Importantly, untreated *hai1a*^{hi2217} mutants displayed elevated activities of the respective inhibitor substrates, as revealed by increased numbers of phospho-EGFR (pEGFR)–positive skin cells (Fig. 2, A′, B′, and H) and increased phosphorylation of the mTORC1 downstream target RPS6 (Fig. 2 I) compared with sibling controls. This indicates that EGFR and mTORC1 act downstream of Matriptase to regulate epidermal homeostasis. Furthermore, *par2b* MO and PD168393 treatment normalized both pEGFR (Fig. 2, B′, C′, D′, and H) and pRPS6 levels (Fig. 2 I), while rapamycin only rescued pRPS6 (Fig. 2 I), but not pEGFR levels (Fig. 2, B′, F′, and H), indicating that mTORC1 acts downstream of Par2b and EGFR.

But how does EGFR activate mTORC1? Three formerly described mediators are the phosphatidylinositol-3-kinase (PI3K)/

Downloaded from http://rupress.org/jcb/article-pdf/219/2/e201905190/1622245/jcb_201905190.pdf by guest on 05 December 2025

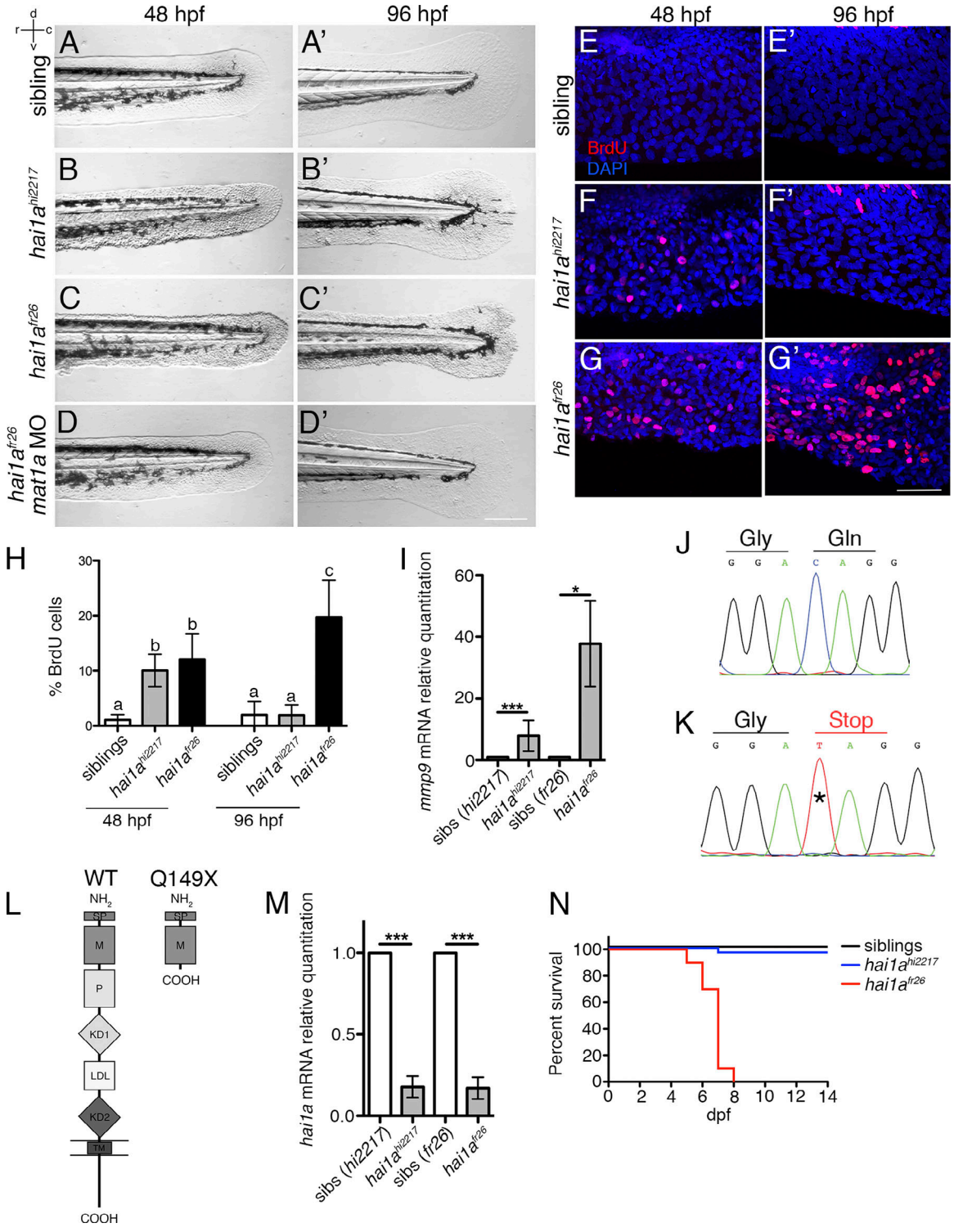

Figure 1. **The skin phenotype of zebrafish *hai1a*^{hi2217} mutants heals spontaneously. (A–D)** Bright field images of embryo tails at 48 (A–D) and 96 hpf (A′–D′). Both the *hai1a*^{hi2217} and the *hai1a*^{fr26} alleles show epidermal aggregates at 48 hpf (B and C), but while the *hai1a*^{hi2217} phenotype has begun to heal spontaneously by 96 hpf (B′), the *hai1a*^{fr26} allele continues to worsen (C′). A morpholino targeting *mat1a* rescues the *hai1a*^{fr26} phenotype at 48 and 96 hpf (D and D′). See also Fig. S1. **(E–G)** Representative maximum intensity projection images of proliferation marker BrdU (red) in the caudal fin fold at 48 hpf (E–G) and 96 hpf (E′–G′). See also Fig. S1. **(H)** Quantification of cell proliferation in the caudal fin fold of embryos at 48 hpf and 96 hpf, in relation to the total number of DAPI-positive nuclei. *n* = 8–20 embryos per condition. **(I)** Q-RT-PCR of *mmp9* at 48 hpf, indicating an increase in transcript levels in the *hai1a*^{fr26} allele compared with the *hai1a*^{hi2217} allele. *n* = 40 pooled embryo tails. **(J and K)** Sanger sequencing chromatograms of WT (J) and *hai1a*^{fr26} (K) genomic DNA, with the nonsense C > T mutation indicated (*). **(L)** Schematic of the zebrafish Hai1a protein and the putative truncated protein produced by the *hai1a*^{fr26} allele. SP, signal peptide; M, MANEC (motif at N terminus with eight cysteines) domain; P, PKD (repeats in polycystic kidney disease 1); KD1, Kunitz domain 1; LDL, low density lipoprotein receptor class A; KD2, Kunitz domain 2; TM, transmembrane domain. Domains were predicted using National Center for Biotechnology Information's

Downloaded from http://rupress.org/jcb/article-pdf/219/2/e201905190/1622245/jcb_201905190.pdf by guest on 05 December 2025

Conserved Domain Database (Marchler-Bauer et al., 2017) and DAS-TM filter (Cserzö et al., 2002). **(M)** Q-RT-PCR of *hai1a* at 48 hpf, demonstrating likely nonsense-mediated decay of the transcript in both *hai1a* mutants. *n* = 40 pooled embryo tails. **(N)** Survival curves comparing siblings (black), *hai1a*^{hi2217} mutants (blue) and *hai1a*^{fr26} mutants (red). *n* = 30 fish. Values represent means ± SD. Significances in (H) were determined via a one-way ANOVA and Tukey's post hoc test. Different letters indicate statistically significant differences ($P < 0.05$). Significances in I and M were determined with a two-tailed Student's *t* test, *, $P < 0.05$; **, $P < 0.01$; ***, $P < 0.001$. Scale bars, 200 µm in A–D and 50 µm in E–G.

AKT and Ras/MEK/pERK pathways, both with positive effects, and the negative regulator AMPK (Davis et al., 2014; Saxton and Sabatini, 2017; Szabo and Bugge, 2011). However, neither pAKT nor pERK levels were elevated in *hai1a*^{hi2217} mutants (Fig. S2, A and B), and mutant skin defects remained unaltered upon chemical interferences with any of the three pathways (Anastasaki et al., 2012; Fig. S2, C–I). As a fourth mechanism, EGFR has been reported to activate mTORC1 by recruitment and activation of PLD (Slaaby et al., 1998). PLD converts phosphatidylcholine to the bioactive signaling lipid and cell membrane component phosphatidic acid (PA), which binds and activates mTOR (Ballou et al., 2003; Fang et al., 2001). Strikingly, inhibition of PLD by 5-fluoro-2-indolyl des-chlorohalopemide (FIPI; Scott et al., 2009), or inhibition of PA production by treatment with butanol (Siddhanta et al., 2000), strongly alleviated the morphological skin defects of *hai1a*^{hi2217} mutants (Fig. 2, E and G) and normalized keratinocyte proliferation levels (Fig. 2, E′′ and J). Furthermore, PLD inhibition normalized pRPS6 levels (Fig. 2 I), but had no effect on EGFR activation (Fig. 2, E′ and H), in line with a function of PLD upstream of mTORC1 and downstream of Matriptase and EGFR. To provide direct evidence for the latter notion, we investigated the sub-cellular localization of PA in basal keratinocytes using transient transgenic expression of a GFP-tagged PA-binding biosensor (*krt19:EGFP-PASS*). As expected for a positive regulation of PLD and PA by Matriptase, GFP-PASS was enriched at plasma membranes of *hai1a*^{hi2217} mutants compared with sibling controls (Fig. 2, K, L, and O; and Fig. S3 J), an effect that was abolished upon FIPI application and EGFR inhibition with PD168393 (Fig. 2, M–O). Together, these results point to a role of PLD-produced PA in a linear Par2b–EGFR–PLD–mTORC1 pathway to mediate the Matriptase-1–induced hyperproliferation in the epidermis of *hai1a*^{hi2217} mutant embryos.

Loss of Matriptase inhibition leads to apical cell extrusion of peridermal and basal keratinocytes

But what contributes to the later spontaneous healing of *hai1a*^{hi2217} mutants, and is this effect mediated by the same pathway? Apoptotic and programmed necrotic cell death seems unlikely, as in 48 hpf *hai1a*^{hi2217} mutant embryos, the numbers of epidermal cells positive after TUNEL, acridine orange staining, and Sytox staining were as low as in WT siblings (Fig. S3, A–I), in line with previous reports (Mathias et al., 2007). Interestingly, however, cells presumably shed from the surface of the skin had been observed within the perivitelline space of *hai1a*^{hi2217}mutant embryos shortly before hatching (36 hpf; Carney et al., 2007). Cryosections through the skin of *Tg(krt4:GFP);Tg(p63:dsRed)* double transgenic *hai1a*^{hi2217} embryos revealed that both *krt4:GFP*-positive peridermal cells (Fig. 3 B) and *p63:dsRed*-positive basal cells (Fig. 3 C) of the bilayered epidermis protruded from the surface. Actin was concentrated below the departing cell, creating rosettes formed by the neighboring peridermal cells most likely forming a contractile ring contributing to the apical displacement of the departing cell (Fig. 3, B–D; and Video 1). This is characteristic of apical cell extrusion (Rosenblatt et al., 2001), a tumor-suppressive process occurring in overcrowded and neoplastic epithelia, including the periderm of zebrafish embryos (Eisenhoffer et al., 2012; Gu et al., 2015; Schepis et al., 2018).

Apical extrusion of basal keratinocytes involves their entosis-like engulfment by peridermal cells

Strikingly, extruding basal keratinocytes were always enveloped by extruding single peridermal cells (Fig. 3, C and E). This ingestive cell behavior strongly resembles entosis found in epithelial cancer cell lines, during which an epithelial cell is engulfed by a neighboring host cell, driven by an active displacement of the "loser" cell into the "winner" cell. Within the host cell, the engulfed cell either dies via lysosomal-mediated degradation or remains alive, and sometimes even divides and eventually escapes the host (Overholtzer et al., 2007; Krishna and Overholtzer, 2016). In zebrafish *hai1a*^{hi2217} mutants, injection of membrane-bound *krt4:TomatoCAAX* (peridermal cells) and *p63:GFPCAAX* (basal cells) indicated that the membrane of the engulfed basal cell is intact and fully surrounded by a membrane of the peridermal host cell (Fig. 3 F). Furthermore, labeling of single basal cells with *p63:lifeact-Ruby* at slightly earlier stages of the engulfment process revealed actin concentration at the rear of the cell (Fig. 3 G), indicative of its own active participation in the engulfment process, as described for entosis in vitro (Florey et al., 2011; Overholtzer et al., 2007; Purvanov et al., 2014). Pharmacological inhibition of the Matriptase signaling pathway, as shown to rescue skin morphology of *hai1a* mutants (Fig. 2 G), significantly reduced not only the number of epidermal rosettes (as indicators of extrusive events; Fig. 3 D), but also the number of basal cells within such rosettes (Fig. 3 H).

Extruded cells could also be recovered from the incubation medium. In line with the in vivo data (Fig. 3 H), numbers of extruded cells in *hai1a*^{hi2217} mutants were over 25 times increased compared with WT embryos, while pharmacological inhibition of the Matriptase signaling pathway significantly reduced the numbers of extruded cells (Fig. 4 F).

To gain more insight into the fate of entosed basal cells, we analyzed shed cells from the incubation medium of *krt4:GFP;p63:dsRed hai1a*^{hi2217} mutants. 89% of recovered cells were single peridermal cells (Fig. 4 A), while the remaining 11% were clusters of peridermal cells containing basal keratinocytes. In those, different patterns of basal cell ingestion were observed, with clusters containing either single (Fig. 4 B) or multiple basal and peridermal cells (Fig. 4, C and D), and with basal cells located

Downloaded from http://rupress.org/jcb/article-pdf/219/2/e201905190/1622245/jcb_201905190.pdf by guest on 05 December 2025

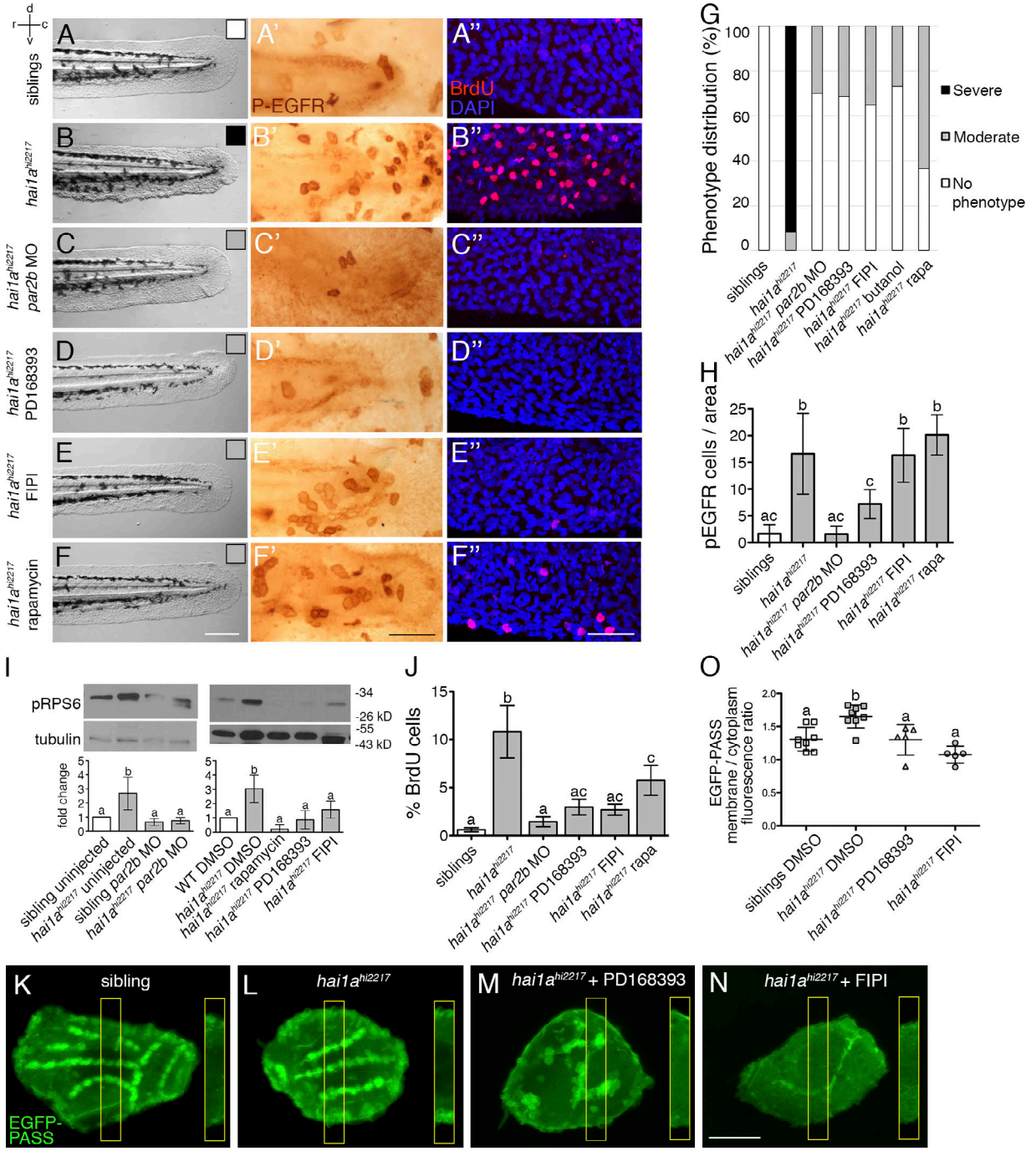

Figure 2. **Loss of Matriptase inhibition activates Par2b-EGFR-PLD-mTORC1 pathway. (A–F)** Representative bright field images of the caudal fin fold at 48 hpf. *hai1a*^{hi2217} embryos were treated with vehicle (B), a morpholino targeting *par2b* (C), or inhibitors of EGFR (PD168393, D), PLD (FIPI, E), or mTORC1 (rapamycin, F). White, gray, and black boxes correspond with the phenotypic classes No phenotype, Moderate, and Severe, respectively, as shown in G. See also Fig. S2. **(A′–F′)** Representative images of anti-pEGFR staining (brown) in the caudal fin fold. **(A′′–F′′)** Representative maximum intensity projection images of BrdU labeling (red) in the caudal fin fold. **(G)** Distributions of the morphological phenotypes in treated embryos, scored according to severity of the phenotype. *n* = 32–50 embryos per condition in two independent experiments. **(H)** Quantification of the numbers of pEGFR-positive cells in A′–F′, in relation to the total area of the fin fold. *n* = 5–9 embryos. **(I)** Representative immunoblots of pRPS6 levels in *par2b* morpholino-injected or inhibitor-treated embryos. *n* = 20 pooled tails per condition. Quantification below each blot indicates the average ratios of each pRPS6 band, normalized against tubulin and relative to the sibling control, calculated from at least three independent experiments. **(J)** Quantification of numbers of BrdU-positive cells in A′′–F′′ relative to the total number of nuclei. *n* = 7–15 embryos. **(K–N)** *krt19:EGFP-PASS* transient expression to visualize PA localization in basal keratinocytes of control siblings and *hai1a*$^{hi2217-}$ mutants. Maximal intensity projections and single planes of boxed regions (insets, same magnification), as used for the determination of relative membrane-cytoplasm values shown in O. See also Fig. S2 J. **(O)** Quantification of EGFP-PASS localization to lateral membranes. Ratios of fluorescence in the proximity of the cell membranes versus the cytoplasm were determined as demonstrated in Fig. S2 J. *n* = 5–8 cells. For quantifications and statistical significances, see legend of Fig. 1. Scale bars in A–F, 200 µm; in A′–F′′, 50 µm; and in K–N, 10 µm.

Downloaded from http://rupress.org/jcb/article-pdf/219/2/e201905190/1622245/jcb_201905190.pdf by guest on 05 December 2025

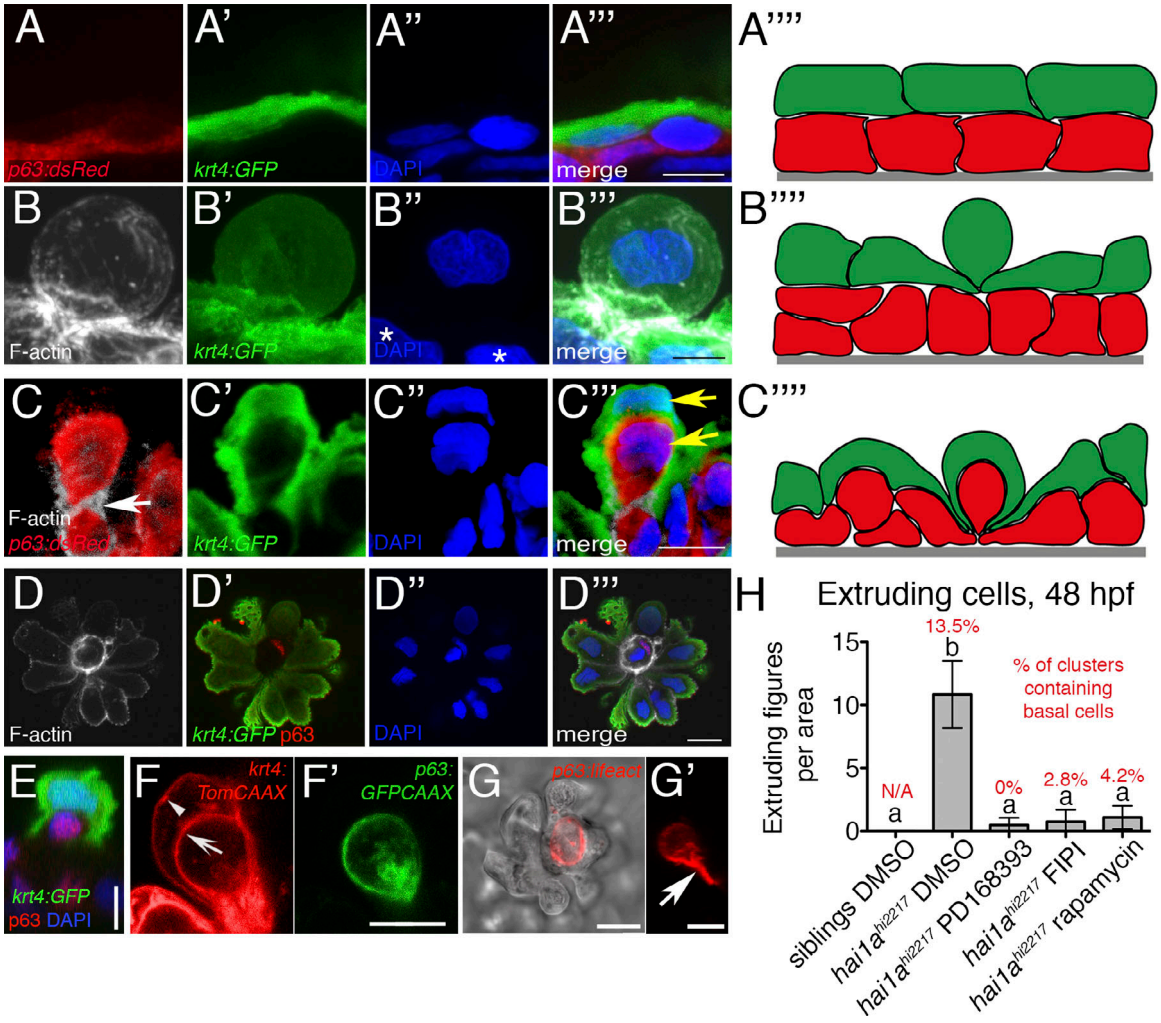

Figure 3. **Loss of Matriptase inhibition leads to apical cell extrusion of peridermal and basal keratinocytes, accompanied by engulfment of basal cells in the epidermis. (A)** WT sibling, (B–G) *hai1a*^{hi2217}mutants at 48 hpf. **(A)** Transverse cryosection image of regular bilayered epidermis with outer *krt4:GFP* peridermal layer labeled in green and *p63:dsRed* basal keratinocytes in red. **(B)** Cryosection image of extruding peridermal cell (green) separating from the surface of the epithelium. Note the F-actin accumulation at the base of the extruding cell (white). Asterisks in B'' indicate nuclei of cells within the plane of the rest of the epidermis. **(C)** Cryosection image of extruding basal cell (red), engulfed by overlying peridermal cells (green); white arrow in C indicates F-actin accumulation (white) at base of engulfed cell (compare with D). Yellow arrows in C''' indicate peridermal and basal cell nuclei. **(D)** En face whole-mount image of an extruding basal cell (red; p63 antibody) in the epidermis, in the center of an F-actin ring (white) formed by surrounding peridermal cells (green). Single plane image; see also Video 1 for the full z-stack. **(E)** YZ orthogonal view of confocal z-stack depicting single peridermal cell (green) engulfing a basal keratinocyte (red; p63 antibody). The *krt4:GFP* plasmid was injected into fertilized eggs to label single peridermal cells. **(F)** Live image of embryo injected at the single-cell stage with *krt4:TomatoCAAX* and *p63:GFPCAAX* constructs, showing intact cell membrane of engulfed basal keratinocytes (F', green), surrounded by cell membrane of host peridermal cell (F, red, arrow). Arrowhead in F points to cell membrane at the surface of host cell. **(G)** Live image of embryo injected at the single-cell stage with *p63:lifeact-Ruby* (red) construct to label single basal keratinocytes, showing actin accumulating at rear of invading basal cell (G'; orthogonal view) located within extruding cell cluster (G, en face view). **(H)** Quantification of rosette-like figures (extrusion events) in median fin folds of untreated and pharmacologically treated *hai1a*^{hi2217}mutants. Percentages of rosettes containing (engulfed) basal cells distal of the peridermal rosette (compare with D) are indicated in red. *n* = 5–7 embryos per condition in two independent experiments. For quantifications and statistical significances, see legend of Fig. 1. Scale bars in A and B, 5 µm; and in C–G, 10 µm.

either completely within a single peridermal cell (entosed, Fig. 4 D, arrow) or within the lumen inside spherical clusters consisting of multiple joined peridermal cells (Fig. 4 D, arrowhead). The diameter of the entosed bodies was consistent with the size of intact basal keratinocytes, and nuclei were visible and intact when stained with the membrane-permeable DNA-binding dye DRAQ5 (Fig. S3 M). Furthermore, labeling with Mitotracker deepRed showed that, at least initially, engulfed basal keratinocytes are alive and metabolically active (Fig. S3 N). In cell culture systems, entosed cells are frequently killed by the host cells in a lysosome-dependent manner (Overholtzer et al., 2007). A dye exclusion assay using trypan blue to label dead cells indicated that the majority of cells are alive at the time of extrusion (Fig. S3 J). However, after 16 h in the incubation medium, approximately one third of engulfed basal cells, but not their host peridermal cells, were Lysotracker positive, pointing to their lysosomal acidification by the host cell (Fig. 4, G and I). In contrast, engulfed basal cells still contained within skin

Downloaded from http://rupress.org/jcb/article-pdf/219/2/e201905190/1622245/jcb_201905190.pdf by guest on 05 December 2025

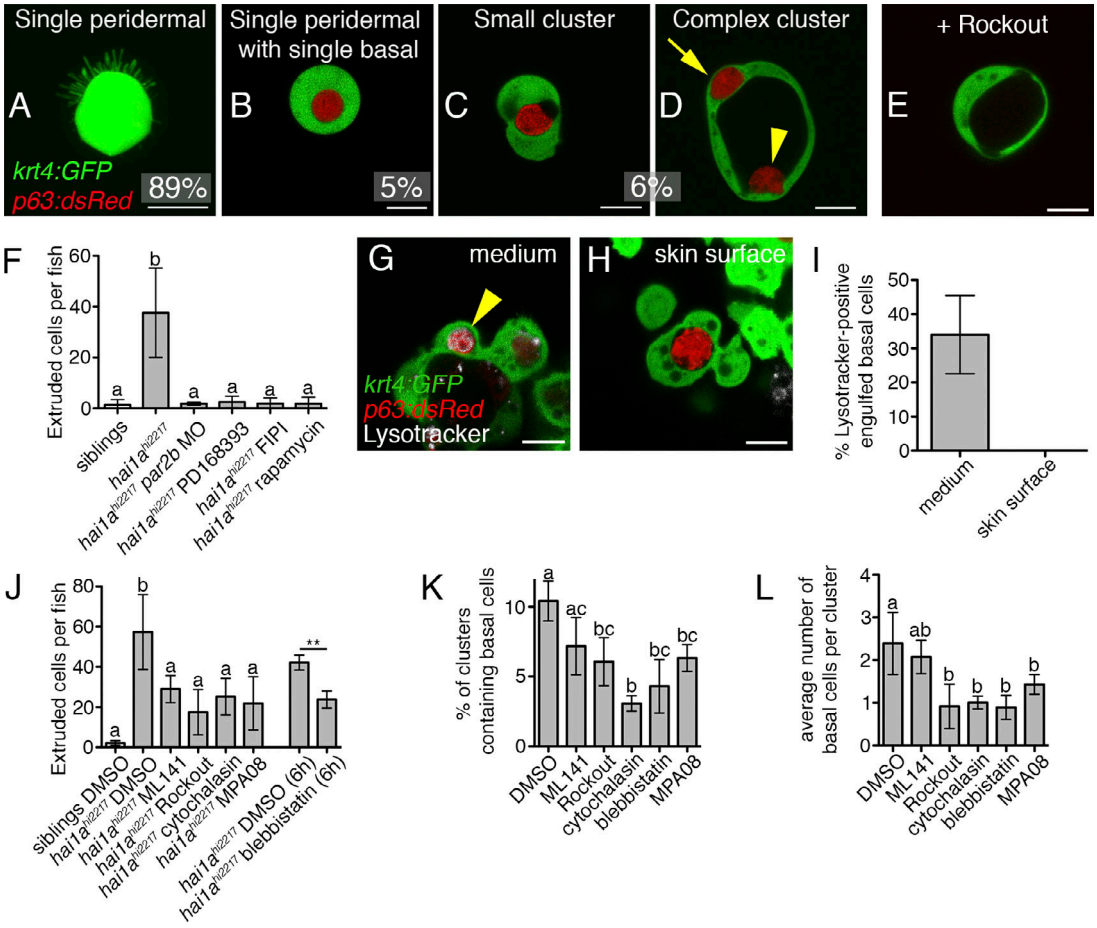

Figure 4. **Inhibition of apical cell extrusion mechanisms also affects entosis. (A–E)** Representative examples of live cells recovered from the embryo medium of *krt4:GFP;p63dsRed hai1a*^{hi2217} embryos at 48 hpf, and quantification of their frequency. Note the filopodia extending from the cell in A. In the complex cluster depicted in D, one basal cell is completely within a peridermal cell (arrow), while a second basal cell (arrowhead) sits in a lumen formed by the joined peridermal cells. **(E)** Representative image of a complex peridermal cell cluster lacking basal cells, recovered after overnight treatment with the Rho kinase inhibitor Rockout. **(A)** Maximum intensity projection; (B–E) single plane of a z-stack. *n* = 303 cells/clusters per condition. See also Fig. S3 and Video 2. **(F)** Quantification of the number of cells extruded per fish at 48 hpf after blockage of components of the Matriptase pathway. *n* = 60–88 embryos. **(G–I)** Representative live single-plane images of cell clusters stained with Lysotracker (white, arrow in G) to label lysosomal-acidified cytoplasms, either recovered from the medium after 16 h of incubation (G) or within the skin of *hai1a*^{hi2217} embryos (H). **(I)** Quantification of Lysotracker-positive engulfed basal cells on skin surface and in incubation medium. *n* = 64 basal cells (medium) or 5 embryos (skin surface). **(J)** Quantification of cells extruded per fish at 48 hpf after 16 h treatment with indicated drugs known to interfere with apical cell extrusion and entosis. To avoid lethal effects of blebbistatin, extruded cells were counted after 6 h of treatment. *n* = 52–79 embryos. **(K and L)** Quantification of the proportion of recovered clusters from J containing basal cells (K), and of the average number of basal cells per cluster (L). *n* = 111–395 cells/clusters. For quantifications and statistical significances, see legend of Fig. 1. Scale bars, 10 µm.

aggregates in vivo were Lysotracker negative (Fig. 4, H and I), indicating that entotic basal cell death is only initiated after cell cluster extrusion.

Of the few known molecular regulators driving the initial engulfment steps of entosis, such as the small GTPase Rho and nonmuscle myosin II, all are also required for apical cell extrusion, largely due to the dependence of both processes on actin-myosin constrictions (Overholtzer et al., 2007; Purvanov et al., 2014; Rosenblatt et al., 2001). In contrast, protrusive activity driven by the small GTPase Cdc42 seems to be specifically required for apical cell extrusions, but not for entosis (Grieve and Rabouille, 2014; Durgan et al., 2017). Accordingly, treatment of *hai1a*^{hi2217} mutants with the Cdc42 inhibitor ML141 only caused a reduction of general apical extrusion rates, while the ratio between extruded peridermal and co-extruded basal cells was not significantly altered. In contrast, treatment with the Rho kinase inhibitor Rockout, the actin polymerization inhibitor cytochalasin D, or the nonmuscle myosin II inhibitor blebbistatin reduced the total number of apically extruded cells (Fig. 4 J), as well as the percentage of clusters containing basal keratinocytes (Fig. 4 K) and the number of basal keratinocytes per cluster (Fig. 4 L). Actually, while cell clusters recovered from the medium of untreated *hai1a*^{hi2217} mutants all contained at least one basal cell (see above; Fig. 4, C and D), treatment with Rockout, cytochalasin, or blebbistatin led to the appearance of clusters containing multiple peridermal but no basal cells (Fig. 4 E). This indicates that in addition to apical cell extrusions, these drugs also specifically inhibit the engulfment of basal by peridermal cells, providing further evidence for the entosis-like nature of this process. Together, these results indicate that epidermal cells

Downloaded from http://rupress.org/jcb/article-pdf/219/2/e201905190/1622245/jcb_201905190.pdf by guest on 05 December 2025

of *hai1a*^{hi2217} mutant embryos undergo trans-layer entosis, and that peridermal cells and entosed basal keratinocytes are shed from the skin's surface. Thus, it appears that elevated Matriptase-1 activity, in addition to its initial induction of epidermal hyperplasia, via the same pathway also activates apical extrusion of peridermal and entosed basal keratinocytes as a tumor-suppressive mechanism underlying the later self-healing of the *hai1a*^{hi2217} mutants.

Apical cell extrusion is promoted by Mmp9 and loss of basement membrane integrity

Even during early developmental stages, outer peridermal cells are normally attached to each other and to underlying basal cells, while basal cells are bound to the underlying basement membrane (Carney et al., 2010; Sonawane et al., 2005; Webb et al., 2007). This suggests that apical cell extrusion and the accompanying entosis must involve mechanisms to loosen such cell–cell and cell–ECM interactions, and that these mechanisms are enhanced in *hai1a*^{hi2217} mutants. Binding of basal keratinocytes to the basement membrane requires a physical interaction between laminins of the basement membrane and integrin receptors on the basal side of basal keratinocytes, which secondarily also affects cell–cell adhesiveness between keratinocytes. For the embryonic zebrafish skin, this is exemplified by the compromised epidermal integrity of zebrafish mutants in the integrin gene *itga3* and the laminin gene *lama5* (Carney et al., 2010; Webb et al., 2007). Indeed, *hai1a*^{hi2217} mutants display a discontinuous distribution of laminin underneath the epidermis (Fig. 5, A and B). Furthermore, *hai1a* displays a tight genetic interaction with *itga3* and *lama5*, as revealed by the synergistic enhancement of both the morphological skin defects and the apical cell extrusion rates caused by the coinjection of low/sub-phenotypic doses of the respective MOs (Fig. 5, C–S), whereas full knockdown of *lama5* or *itga3* alone had no effect on cell extrusion rates (Fig. 5, R and S). Matriptase could possibly contribute to the loss of laminin-dependent cell adhesiveness via matrix metalloproteases like Mmp2 or Mmp9, gelatinases with laminin-5 as a described substrate (Giannelli et al., 1997; Zhang et al., 1991). Indeed, *mmp9* expression is up-regulated in *hai1a* mutants (Fig. 1 I) in a Par2b-, EGFR-, PLD-, and mTORC1-dependent manner (Fig. 5 T), while treatment with a chemical Mmp9/13 inhibitor led to a significant reduction in apical cell extrusion rates in *hai1a* morphants (Fig. 5 Q and Fig. 6 I) and in embryos coinjected with low amounts of *hai1a* and *lama5* MOs or *hai1a* and *itga3* MOs (Fig. 5, R and S). This normalization, however, was less pronounced than the effect caused by injected *mat1a* MO (Fig. 5, H, L, and P–S). This suggests that Matriptase-1 might promote laminin degradation and thereby apical cell extrusion rates by transcriptional activation of *mmp9* via the Par2b–EGFR–PLD–TORC1 pathway, and possibly also by direct laminin degradation, consistent with former in vitro data (Tripathi et al., 2011). Our observation that full *lama5* and *itga3* morphants/mutants per se (Carney et al., 2010; Webb et al., 2007) lack apical cell extrusion further indicates that these mechanisms to destabilize cell adhesiveness are necessary, but not sufficient, for apical cell extrusion. This points to the coexistence of additional effectors of Matriptase-1 to induce apical cell extrusion.

Entosis, apical cell extrusion, and self-healing in the *hai1a*^{hi2217} mutant are mediated by S1P signaling

Apical cell extrusion has formerly been shown to be driven by the signaling lipid molecule S1P (Gu et al., 2011; Gu et al., 2015), which is produced in cellular membranes by sphingosine kinases. Interestingly, it is also known that PA can recruit sphingosine kinase 1 (Sphk1) to cell membranes (Delon et al., 2004), providing a possible mechanistic link between the Matriptase mediator PLD and the elevated apical cell extrusion rates. Indeed, in basal keratinocytes of *hai1a*^{hi2217} mutants, transiently expressed, GFP-tagged mouse Sphk1 (*krt19:EGFP-Sphk1WT*) displayed a more pronounced membranous/cortical localization than in WT siblings (Fig. 6, C, D, and G). This cortical localization was dependent upon PA and abolished by treatment with the PLD inhibitor FIPI (Fig. 6, E and G), whereas treatment with rapamycin to inhibit mTORC1 did not alter Sphk1 localization (Fig. 6, F and G), pointing to the existence of a branching point in the Mat1a–Par2b–EGFR–PLD pathway at the level of the PLD product PA, with mTORC1 and Sphk1 as downstream mediators that act largely in parallel.

To examine the role of Sphk1-produced S1P in entosis and cell extrusion, we blocked S1P signaling in *hai1a*^{hi2217} mutants, either by treating them with the chemical Sphk1/2 inhibitor MPA08, or by generating double mutants that in addition to Hai1a lack a functional S1P receptor S1pr2 (*s1pr2*^{te273}; Kupperman et al., 2000). Indeed, compared with untreated *hai1a*^{hi2217} mutants, MPA08-treated single *hai1a*^{hi2217} mutants and *hai1a*^{hi2217};*s1pr2*^{te273} double mutants at 48 hpf showed a significant reduction of overall apical cell extrusion rates (Fig. 4 J and Fig. 6 H), and of the presence of entosed basal cells within remaining extruded cell clusters (Fig. 4, K and L). Consistently, in the skin of mutant embryos in vivo, the number of actin rosettes indicative of extrusive processes was reduced upon MPA08 treatment (Fig. 6, I–K). Such blockage of entosis and cell extrusion was accompanied by a failure to recover body morphology (Fig. 6, L′–O′; and Fig. S4, A–D) and to normalize epidermal proliferation rates, which remained high even at 96 hpf (Fig. 6, L′′–O′′′ and Q). Together, this indicates that S1P and its receptor S1pr2 act downstream of PLD to mediate entosis and apical cell extrusion. This extrusion machinery preferentially targets proliferative keratinocytes, leading to a strong reduction in epidermal proliferation rates and to spontaneous healing of the epidermal defects of *hai1a*^{hi2217} mutants between the second and fourth day of development.

Similarly high epidermal proliferation rates and strong morphological defects of the epidermis at 96 hpf as upon blockage of S1P signaling were obtained upon long-term treatment of *hai1a*^{hi2217} mutants with the PLD inhibitor FIPI (Fig. 6, P–P′′′ and Q), despite the alleviation of these defects this treatment had caused at 48 hpf (Fig. 2). This suggests that blockage of Matriptase signaling upstream of the branching point, affecting both the preneoplastic mTORC1 and the tumor-suppressive S1P branch, only leads to a transient alleviation of epidermal hyperplasia and dysmorphology, possibly because of predominant suppression of mTORC1-mediated hyperplasia early, but predominant suppression of entosis and apical cell extrusions during later stages.

Downloaded from http://rupress.org/jcb/article-pdf/219/2/e201905190/1622245/jcb_201905190.pdf by guest on 05 December 2025

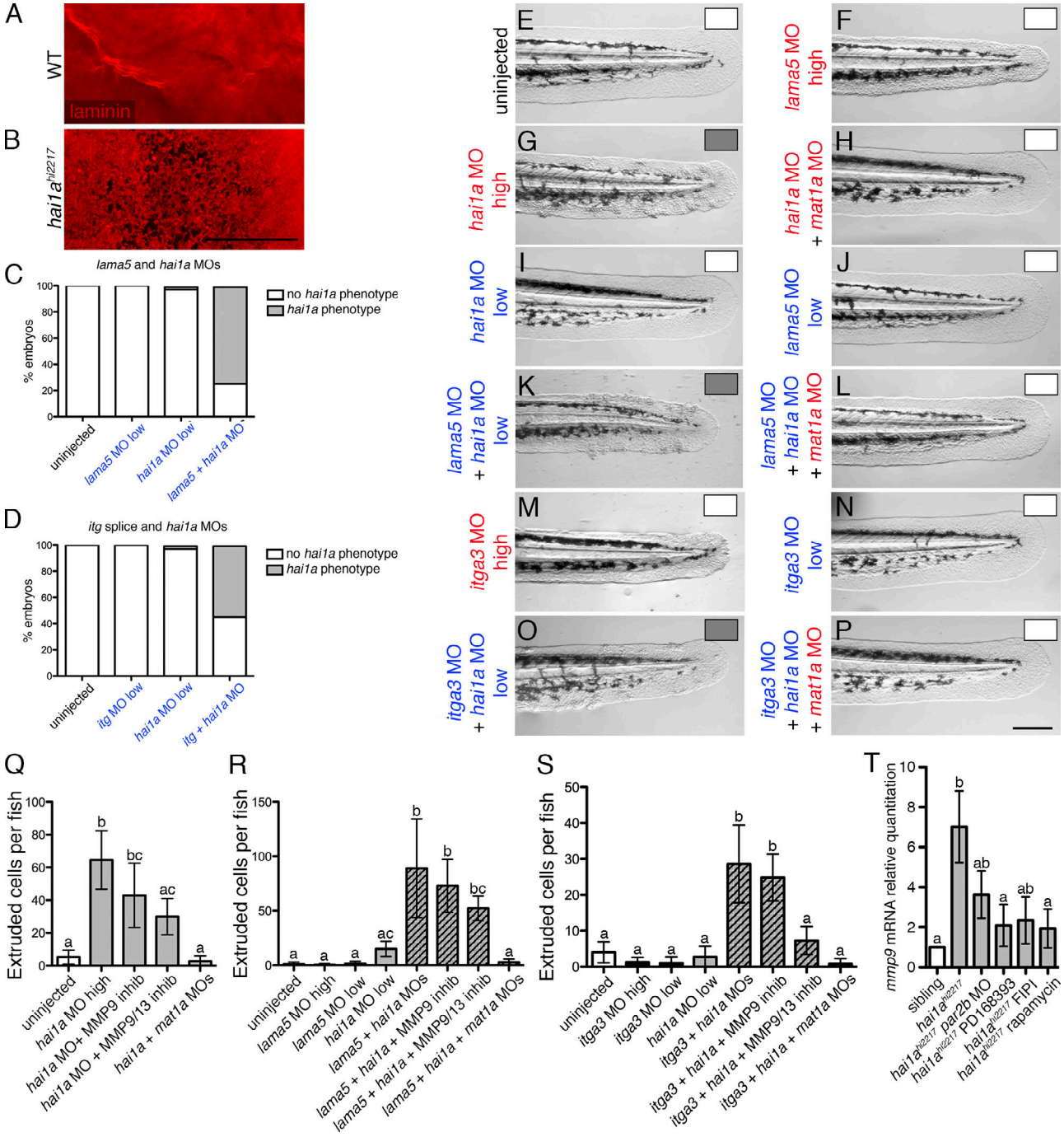

Figure 5. **Apical cell extrusion is promoted by Mmp9 and loss of basement membrane integrity. (A and B)** Laminin antibody staining (red) in the caudal fin fold revealing compromised basement membrane integrity in *hai1a*^{hi2217} embryos at 48 hpf. **(C)** Genetic interaction between *lama5* and *hai1a*. Sub-phenotypic/low doses of single morpholinos had no effect on the morphological phenotype, but combined injection of sub-phenotypic doses recapitulated the *hai1a* epidermal phenotype. *n* = 99 or 100 embryos per condition. **(D)** Genetic interaction between *itga3* and *hai1a*. *n* = 100 embryos. **(E–P)** Representative bright field images of single and combined morpholino injections at 48 hpf. Note that the *mat1a* MO fully rescues the epidermal phenotype (H, L, and P). **(Q–S)** Quantification of cell extrusions at 48 hpf for the *hai1a* morphants (Q) and the genetic interaction between *lama5* and *hai1a* (R) and *itga3* and *hai1a* (S). The cell extrusion phenotype depends in part on Mmp9 and Mmp13, and is fully rescued upon coinjection of the *mat1a* morpholino. *n* = 40–178 embryos. **(T)** Q-RT-PCR demonstrating that levels of *mmp9* in mutants are reduced upon treatment. *n* = 40 pooled embryo tails. For quantifications and statistical significances, see legend of Fig. 1. Scale bars in A and B, 20 µm; in E–P, 200 µm.

Downloaded from http://rupress.org/jcb/article-pdf/219/2/e201905190/1622245/jcb_201905190.pdf by guest on 05 December 2025

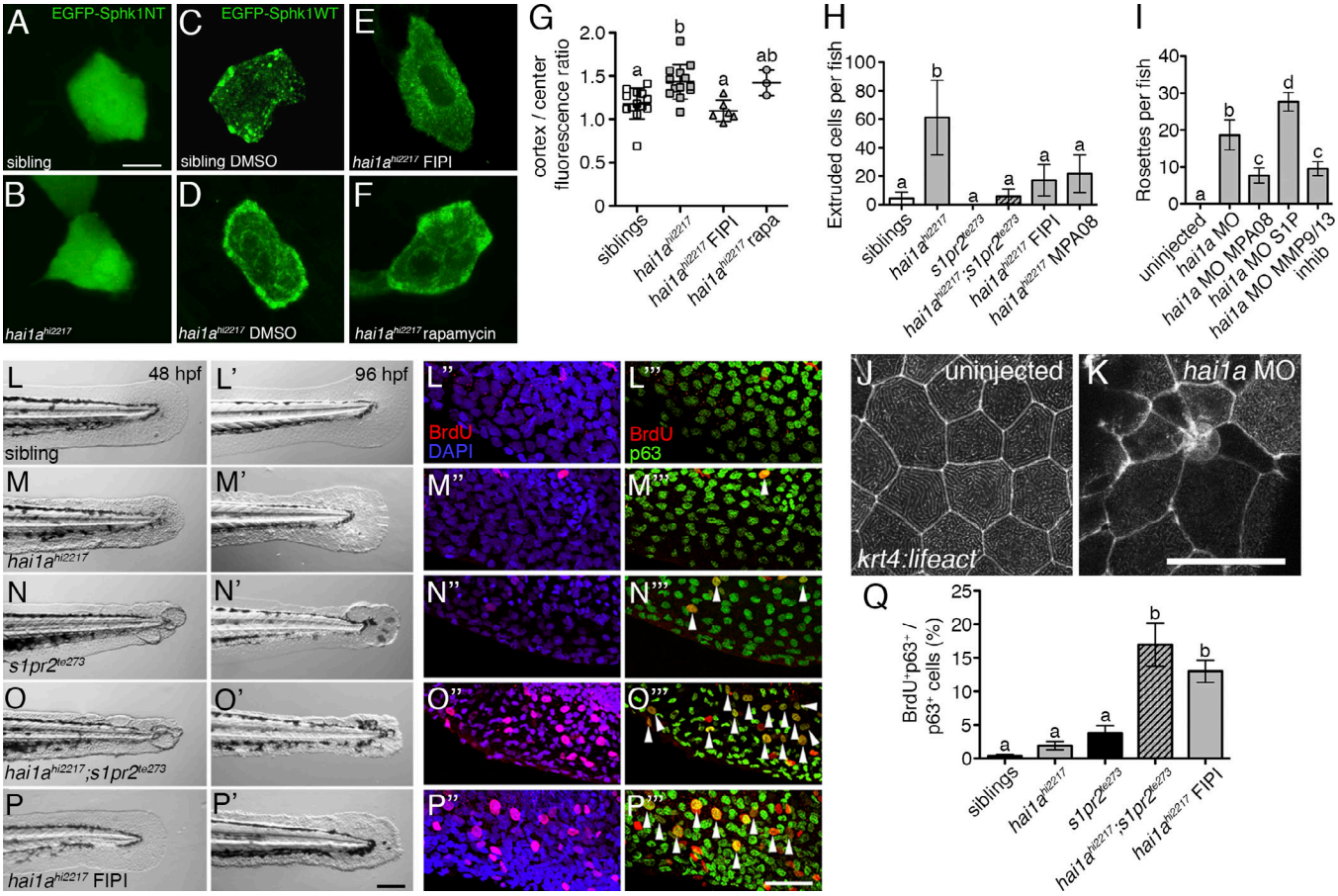

Figure 6. **Apical cell extrusion and self-healing in the *hai1a*^{hi2217} mutant are mediated by S1P signaling. (A–F)** Localization of transgene encoded, transiently expressed, and EGFP-tagged WT mouse Sphk1 (*krt19:EGFP-Sphk1WT*; C–F) and, as negative control, a C-terminally truncated version of Sphk1 lacking the PA-binding site (*krt19:EGFP-Sphk1NT*, A and B) in single basal keratinocytes of zebrafish WTs or *hai1a*^{hi2217} mutants at 48 hpf. **(G)** Quantification of Sphk1 cortical localization, determined as the ratio of average cortical fluorescence measured in a radius of 2 µm from the cell border, to the average fluorescence in the interior of the cell. *n* = 3–13 cells per condition. **(H)** Quantification of cell extrusion numbers at 48 hpf upon blockage of S1P signaling, either by mutation of the *s1pr2* gene or by sphingosine kinase inhibition (MPA08), or upon FIPI treatment upstream of the S1P pathway. *n* = 19–39 embryos. **(I–K)** Alternative method of quantification of extruded cell numbers, counting the number of actin rosettes per embryo tail in *krt4:lifeact-ruby* (white in J and K) *hai1a* morphants upon drug treatment. *n* = 6–8 embryos. **(L–P and L′–P′)** Bright field images of embryo tails at 48 hpf and 96 hpf, showing that blockage of cell extrusion in *hai1a*^{hi2217} mutants, either by *s1pr2* mutation or by continual FIPI treatment from 10–96 hpf, leads to worsening of the epithelial phenotype over time (compare M′ with O′ and P′). See also Fig. S4. **(L′′–P′′ and L′′′–P′′′)** BrdU (red) incorporations at 96 hpf demonstrate increased proliferation rates upon blockage of cell extrusion. Double BrdU and p63 (green) labeling reveals proliferating basal keratinocytes (arrowheads in L′′′–P′′′). **(Q)** Quantification of proliferation rates of basal keratinocytes at 96 hpf after blockage of apical cell extrusion. *n* = 7–16 embryos. For quantifications and statistical significances, see legend of Fig. 1. Scale bar in A–F, 10 µm; in L–P′, 200 µm; and in J, K, and L′′–P′′′, 50 µm.

Combinatorial PLD inhibition and S1P administration to reactivate apical cell extrusions can heal the otherwise lethal amorphic *hai1a* ^{fr26} allele

Having identified S1P-dependent entosis and apical cell extrusion as the compensatory, tumor-suppressive side of Matriptase function accounting for the later self-healing of *hai1a*^{hi2217} mutants, we turned back to the amorphic $^{hai1a^{fr26}}$ allele, which does not heal spontaneously and displays persistent epidermal hyperplasia. Reasoning that this might be due to an imbalance between the pro-proliferative and tumor-suppressive branches, we tested whether stronger activation of apical extrusion by treatment with S1P might be beneficial for *hai1a*^{fr26} mutants. Similar to the results reported above for the weaker *hai1a*^{hi2217} allele, *hai1a*^{fr26} mutants treated with FIPI from 24 hpf onwards displayed a strong reduction in apical cell extrusion at 48 hpf, whereas administration of S1P led to a twofold increase (Fig. 6 I and Fig. 7 B), suggesting that S1P might be able to compensate for the negative, extrusion-blocking side effects of FIPI. However, former studies had revealed a mitogenic effect of S1P (Zhang et al., 1991), which would be counterproductive here. And indeed, S1P increased proliferation rates in both mutant and sibling embryos when applied early and for 4 d (24–120 hpf). In contrast, no such mitogenic effect was observed upon shorter/later treatments for 2 d (72–120 hpf; Fig. S4, E–M). This indicates that proper timing is absolutely crucial for S1P treatments. Therefore, also taking into account the time courses of self-healing and FIPI effects in the weak *hai1a*^{hi2217} allele, we progressed to a combinatorial treatment regimen, treating *hai1a*^{fr26} mutants from 24 to 72 hpf with FIPI to attenuate keratinocyte proliferation (compare with Fig. 2 J for *hai1a*^{hi2217}), followed by administration of S1P from 72 hpf, when *hai1a*^{hi2217} mutants

Downloaded from http://rupress.org/jcb/article-pdf/219/2/e201905190/1622245/jcb_201905190.pdf by guest on 05 December 2025

begin to recover, through 120 hpf to promote apical cell extrusion (Fig. 7, A and B). This extrusion-promoting effect of S1P was most likely not due to changes in cell–matrix or cell–cell adhesions, as we did not observe any differences in laminin and E-cadherin abundance and distribution upon S1P treatment from 72–120 hpf (Fig. S4, N–U). Assessment of embryos at 120 hpf revealed that the sequential treatment led to a reduction of epidermal proliferation rates and an efficient rescue of the overall skin morphology to almost WT conditions, while the effects of single treatments using the same temporal regimen were rather minor (Fig. 7, C–S). Furthermore, while untreated and singly treated mutants began dying shortly after 3 dpf, mutants with the combined treatment survived to the end of the treatment (5 dpf) and even beyond 8 dpf (Fig. 7, T and U). Similar treatment regimens using rapamycin and S1P were less successful (Fig. S5). While rapamycin alone reduced cell proliferation in *hai1a*^{fr26} mutants (Fig. S5, C, M, and O), long-term survival of these embryos was impaired (Fig. S5 U), most likely due to side effects of rapamycin on the development of the zebrafish embryo, resulting in failed swim bladder formation even in siblings (data not shown). Of note, in contrast to FIPI and S1P combinatorial treatments, application of S1P following rapamycin had no additional negative effect on cell proliferation at 120 hpf (Fig. S5, C, O, and S) and did not significantly alleviate the developmental defects or lethality of rapamycin-treated mutants (Fig. S5, E, G, J, and U), consistent with our proposed mechanistic model, according to which rapamycin, in contrast to FIPI, does not compromise endogenous S1P production (Fig. 7 V).

These results indicate that enhancement of apical cell extrusion by S1P administration can compensate for the negative side effects of FIPI treatment, restoring the balance between the pro-proliferative and tumor-suppressive branches in the *hai1a*^{fr26} mutant (Fig. 7 V) and resulting in healing of its otherwise lethal skin phenotype.

Discussion

The type two transmembrane serine protease Matriptase is well-studied as an oncogene, and dysregulated Matriptase activity is associated with multiple epithelial cancers (List et al., 2006). Here, we uncovered a previously undescribed pro-proliferative Par2b-EGFR-PLD-mTORC1 signaling axis downstream of Matriptase. Additionally, we exploited the spontaneous healing of the zebrafish *hai1a*^{hi2217} mutant to show that increased Matriptase activity can also trigger a parallel pathway culminating in the S1P-mediated tumor-suppressive mechanism of entosis and apical cell extrusion, revealing a second face for Matriptase. According to the model drawn from our data (Fig. 7 V), these two counteracting pathways branch downstream of the shared Matriptase mediator PLD, with PA promoting the membrane localization and thereby activation of both mTORC1 and sphingosine kinase. The relative strengths and timing by which the tumor-suppressive branch is activated seem to dictate whether or not the organism recovers.

Matriptase as a tumor suppressor

Analyzing the mechanisms by which Matriptase promotes apical cell extrusion, we found them to be at least threefold (Fig. 7 V). First, apical cell extrusion is promoted by hyperplasia-induced cell crowding, consistent with the concomitant alleviation of keratinocyte proliferation and extrusion rates by treating *hai1a* mutants with rapamycin (Fig. 2 J and Fig. 4 F). Second, it is promoted by matrix metalloprotease–induced detachment of basal keratinocytes from the underlying basement membrane (Fig. 5), which also compromises intercellular adhesiveness among keratinocytes, thereby possibly also promoting the shedding of outer keratinocytes (Carney et al., 2010). Of note, this tumor-suppressive effect of Mmp9 is in seeming contrast to its oncogenic effect revealed in another zebrafish skin mutant, where it promotes keratinocyte invasiveness (Hatzold et al., 2016), pointing to a similar double face of matrix metalloproteases as reported here for Matriptase. Finally, the third, and likely most crucial, mechanism to stimulate apical cell extrusion: Matriptase uses S1P signaling, indicated by the absence of cell extrusion upon loss of S1P production or signal transduction (Fig. 6 H), and its promotion upon administration of exogenous S1P (Fig. 7 B). We also elucidated the mechanisms by which elevated Matriptase activity stimulates S1P signaling, showing that Sphk1, which catalyzes the phosphorylation of sphingosine to S1P, displays a PLD-dependent translocation to cortical regions of *hai1a*^{hi2217} mutant keratinocytes (Fig. 6, A–G). This is consistent with reports that membranous PA directly binds cytoplasmic Sphk1, thereby recruiting it to cell membrane compartments (Delon et al., 2004). Plasma membrane localization of Sphk1 in turn would allow the release of S1P into the extracellular space, where it could act in an autocrine and/or paracrine manner to facilitate cell extrusion, in agreement with previous reports of extruding vSrc-transformed cells (Anton et al., 2018).

Cell extrusion of basal cells in the epithelial bilayer is achieved via their entosis-like engulfment by surface cells

Apical cell extrusion has previously only been described for cell monolayers, while here we show that apical extrusion of cells from lower layers takes place as well, at least within a bilayered epithelium. Indeed, for tumor suppression, this loss of basal cells is crucial, as it is the hyperproliferation of such basal cells that mainly contributes to epidermal hyperplasia (Carney et al., 2007; Schepis et al., 2018). Strikingly, however, basal cells were only released from the epithelium when surrounded by peridermal cells (Figs. 3 and 4), presumably as a means to maintain epithelial integrity.

Intriguingly, this process of basal cell engulfment strongly resembles the type IV nonautonomous cell death mechanism entosis, which was first described in cancer cell lines of epithelial origin (Martins et al., 2017; Overholtzer et al., 2007), whereas reports of its in vivo occurrence are scarce (Lee et al., 2019), leaving it largely unclear what role and relevance entosis has in tissue homeostasis and carcinogenesis. It even remains uncertain whether entosis constitutes a tumor-suppressive or tumor-promoting mechanism (Krajcovic et al., 2011; Overholtzer et al., 2007). In the zebrafish *hai1a* mutant, entosis of basal keratinocytes appears to occur only in combination with apical cell extrusion and can therefore be regarded as a tumor-suppressive mechanism. These results could be relevant for

Downloaded from http://rupress.org/jcb/article-pdf/219/2/e201905190/1622245/jcb_201905190.pdf by guest on 05 December 2025

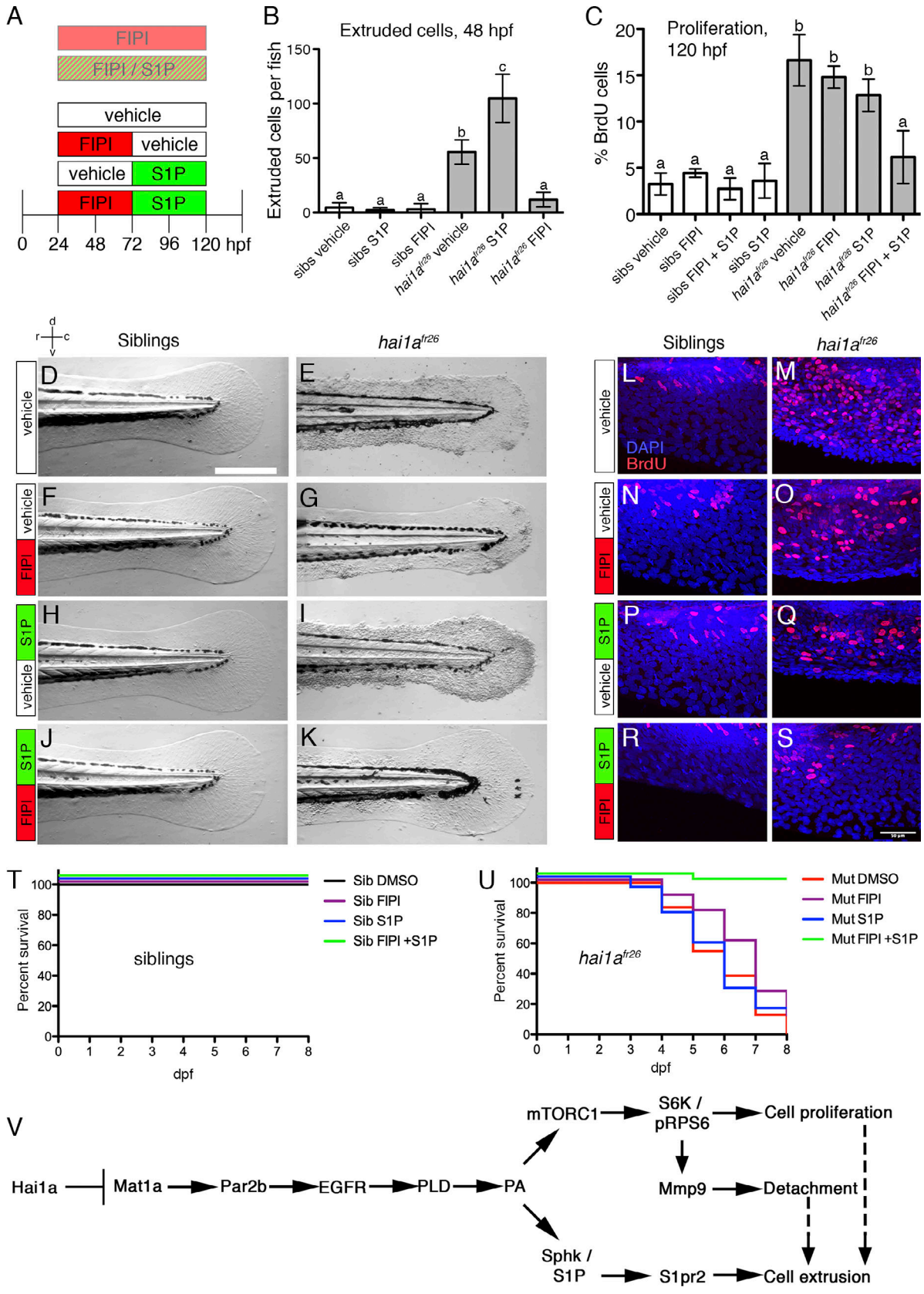

Figure 7. **Combinatorial PLD inhibition and S1P administration to reactivate apical cell extrusion can heal the otherwise lethal *hai1a*^{fr26} allele.** **(A)** Schematic indicating the time course of different drug treatment regimes. Both long-term FIPI and simultaneous FIPI + S1P treatment worsened the epidermal phenotype (not shown). For sequential treatments shown in B–U, embryos were treated with FIPI from 24–72 hpf, followed by S1P treatment from 72–120 hpf. Single treatments occurred in the same time frames as in the combinatorial regimen. **(B)** Quantification of extruded cell numbers at 48 hpf

Downloaded from http://rupress.org/jcb/article-pdf/219/2/e201905190/1622245/jcb_201905190.pdf by guest on 05 December 2025

following individual drug treatments of siblings and *hai1a*^{fr26} mutants from 24 hpf. *n* = 18–30 embryos per condition. **(C)** Quantification of BrdU-positive cells at 120 hpf in embryos treated with FIPI and/or S1P. *n* = 5–11 embryos per condition. **(D–K)** Bright field images of the fin fold of sibling controls and *hai1a*^{fr26} mutants at 120 hpf after indicated treatments. **(L–S)** Representative maximum intensity projection images of BrdU incorporation (red) in 120 hpf embryos after indicated treatments. **(T and U)** Survival curves of drug-treated embryos. *n* = 30 fish per condition. For quantifications and statistical significances, see legend of Fig. 1. Scale bar in D–K, 300 µm; in L–S, 50 µm. **(V)** Model of branched pathway mediating the double face of Matriptase in *hai1a* mutant embryos. For details, see text.

carcinogenesis in mammalian tissues of similar structure, such as the bilayered mammary duct epithelium, which undergoes a similar process of cell extrusion into the lumen, accompanied by cell engulfment by neighboring epithelial cells (Monks et al., 2005, 2008).

Since the molecular mechanisms driving entosis are little understood, the molecular pathway identified here could open up new avenues of enquiry. For example, PLD and PA might be necessary for cell membrane dynamics that take place during entosis, in line with their formerly described roles during macroautophagy and macropinocytosis in phagocytes (Bohdanowicz et al., 2013; Dall'Armi et al., 2010). It remains unclear how peridermal cells specifically recognize and target proliferating basal cells, as indicated by the drop of overall proliferation rates of p63-positive basal cells as a result of the extrusion process (Fig. 6 Q), and in contrast to cell competition wherein loser cells have a proliferative disadvantage (Ellis et al., 2019). Detachment of dividing basal cells from the basement membrane, possibly mediated by matrix metalloproteases, might be involved. Another crucial factor appears to be S1P. For phagocytosis of apoptotic cells, macrophages and neutrophils rely on "find-me" and "eat-me" signals expressed by their targets. Intriguingly, S1P is a "find-me" signal for engulfment by phagocytic cells (Gude et al., 2008). In line with this role, we found that pharmacological inhibition of the S1pr2 reduced not only extrusion rates, but also the ratio of basal cells within the extruded cell clusters (Fig. 4, J and K). This suggests that one and the same signaling molecule, S1P, is responsible for the induction of both the engulfment of basal keratinocytes by overlying peridermal cells and the subsequent extrusion of the resulting cell clusters. Therefore, S1P can be considered as a master regulator of this tumor-suppressive mechanism in the context of a bilayered epithelium.

Implications for potential treatment of Matriptase-dependent carcinogenesis

Given its up-regulation in many types of epithelial-derived cancers, it is crucial to unravel the downstream pathways initiated by Matriptase activity, and to identify druggable targets therein. Both EGFR and mTORC1 inhibitors are well-studied, but known to have adverse side effects in the long term, especially when used as monotherapy (Arasada et al., 2014; Choo et al., 2008; Holcmann and Sibilia, 2015; Huang and Fu, 2015; Martin et al., 2013; Tsaur et al., 2012). In this vein we found that rapamycin treatment had adverse effects (Fig. S5), despite the fact that based on our proposed pathway, it would be the most straightforward treatment, inhibiting cell proliferation without directly compromising tumor-suppressive entosis and apical cell extrusion processes (Fig. 7 V). More recently, both PLD (Bruntz et al., 2014; Henkels et al., 2013; Park et al., 2012; Scott et al., 2009; Su et al., 2009) and Sphk1/S1P (Dany, 2017; Kunkel et al., 2013; Pyne et al., 2011) have become the focus of anti-cancer small-molecule inhibitor development. Our results demonstrate that combinatorial treatments, which take into account bifurcations in the signaling pathway, are likely to be far more effective than monotherapy. This seems to be particularly so when double-face regulators with both oncogenic and tumor-suppressive effects are involved, such as Matriptase, for which we combined blockage of the shared stem of the pathway with a reactivation of the tumor-suppressive branch. Of note, at the concentrations and temporal profiles used, the applied components (FIPI and S1P) only affected mutants, but not WT fish, pointing to an absence of adverse side effects. Similar combinatorial concepts should also be considered for other oncogenes associated with tumor-suppressive properties or vice versa (Ávalos et al., 2014; Lebrun, 2012; Loizou et al., 2019; Rada et al., 2018; Turunen et al., 2017).

Materials and methods

Zebrafish lines

In general, experiments were performed on zebrafish embryos between 2 and 5 dpf, with homozygous mutants compared with unaffected sibling controls unless otherwise indicated. Embryos were kept at 27°C in E3 embryo medium with 2 × 10^{-5}% methylene blue (60× stock: 295 mM NaCl, 10 mM KCl, 20 mM $CaCl_2$, and 20 mM $MgSO_4$), randomly assigned to treatment groups, and no effort was made to separate embryos by sex. Genotype was confirmed using genomic DNA and PCR as below, or by incrossing and subsequent phenotyping. The following zebrafish lines were used: *hai1a*^{hi2217Tg} (Amsterdam et al., 2004; Carney et al., 2007); *krt4*:GFP^{gz7Tg} (periderm labeling; Gong et al., 2002); *tp63:dsRed*^{fr46Tg} (basal cell labeling; construct kindly provided by S. Rieger, University of Miami, Miami, FL; Lisse et al., 2016); *s1pr2* mutant *edg5*^{te273} (Kupperman et al., 2000); *krt4:lifeact-ruby*^{fr47Tg} (this study; see below); *mpx:GFP*^{i114Tg} (neutrophil labeling; Renshaw et al., 2006); and *mpeg1.1:mcherry-F*^{ump2Tg} (macrophage labeling; Bernut et al., 2014). The *hai1a*^{fr26} mutant was recovered from an N-ethyl-N-nitrosourea mutagenesis forward genetics screen performed in the Hammerschmidt laboratory (Carney et al., 2010). All zebrafish experiments were approved by the national animal care committees (Landesamt für Natur, Umwelt und Verbraucherschutz Nordrhein-Westfalen; 8.87–50.10.31.08.129; 84–02.04.2012.A251; City of Cologne; 576.1.36.6.3.01.10 Be) and the University of Cologne.

Genotyping

The *hai1a*^{hi2217} mutants were genotyped by PCR using the following three primers: genotyping primer *hai1a*^{hi2217}_1 (5′-CGACGC TTGTACATCCTGCC-3′), genotyping primer *hai1a*^{hi2217}_2 (5′-ATT TCTGAAAACTGGGCCAC-3′), and genotyping primer *hai1a*^{hi2217}_3

Downloaded from http://rupress.org/jcb/article-pdf/219/2/e201905190/1622245/jcb_201905190.pdf by guest on 05 December 2025

(5′-GCTAGCTTGCCAAACCTACAGGT-3′). Primers 1 and 3 detected the mutant allele with a band of 486 base pairs, while primers 1 and 2 detected the WT allele with a band of 524 base pairs. The *s1pr2*^{te273} mutants were genotyped by PCR using the following primers: genotyping primer *s1pr2*^{te273}_F (5′-CATTTCATTTGACTC CTGTCCAGTG-3′) and genotyping primer *s1pr2*^{te273}_R (5′-TAG TATCGGGTGTTGAGGGGC-3′) followed by digestion using *Ape*KI (NEB), following the protocol detailed by the Zebrafish International Resource Center.

Plasmid constructs and transgenesis

The PA-binding bioprobe GFP-PASS, a kind gift from G. Du (University of Texas Health Science Center, Houston, TX; Zhang et al., 2014), was used to create *krt19:EGFP-PASS* using the Tol2 kit (Kwan et al., 2007). This construct contains the basal cell–specific *krt19* promoter, driving expression of the GFP-tagged PA-binding domain of *Saccharomyces cerevisiae* protein Spo20. Additionally, a nuclear export sequence derived from protein kinase A inhibitor α is added to prevent the nuclear retention of the probe (Zhang et al., 2014). The GFP-PASS bioprobe was cut with EcoRI and BamHI to release it from the vector and to remove the SV40 polyA sequence, gel-purified (Macheray-Nagel), and ligated using T4 ligase (NEB) into EcoRI/BamHI-digested middle entry vector containing a multiple cloning site (pME-MCS). To create *krt19:EGFP-mmSphK1WT* and *krt19:EGFP-mmSphK1NT1*, we used N-terminally GFP-tagged mouse sphingosine kinase WT and deletion (NT1, missing the PA-binding domain) constructs, kindly provided by N. Ktistakis (Babraham Institute, Cambridge, UK; Delon et al., 2004). Both of the sphingosine kinase constructs were released from the backbone using AgeI and XbaI digestion, gel-purified, and ligated into XmaI/XbaI-digested middle entry vector. The basal cell–specific *krt19* promoter has been described previously (Lee et al., 2014). The *krt4:lifeact-ruby* construct was also generated using the Tol2 kit, with the described *krt4* promoter (Gong et al., 2002). The primers 5′-GGGGACAAGTTTGTACAA AAAAGCAGGCTCCACCATGGGTGTCGCAGATTTGATC-3′ and 5′-GGGGACCACTTTGTACAAGAAAGCTGGTTAAGCGCCTGTGCT ATGTC-3′ were used to amplify the *Lifeact-Ruby* cDNA from plasmid zMPO:Lifeact-Ruby (kind gift from A. Huttenlocher, University of Wisconsin-Madison, Madison, WI; Yoo et al., 2010) and cloned into pDONR221 (Invitrogen). The construct was used to generate the stable transgenic line *krt4:lifeact-ruby*^{fr47Tg} by standard injection and screening procedures. To generate *p63:lifeact-ruby*, the *p63* promoter was cut from *p63:dsred* (Lisse et al., 2016) and ligated into the XhoI/BamHI site of a modified pT2AL200R150G vector (Urasaki et al., 2006), in which the *EF1:egfp* sequence had been replaced by a multiple cloning site. The *lifeact-ruby* sequence was amplified using the primers 5′-GATATC AGGCTCCACCATGGGTGTCG-3′ and 5′-GATATCTTAAGCGCC TGTGCTATGTC-3′ and inserted into the *Eco*RV site downstream of the *p63* promoter. To generate *p63:GFP-CAAX*, a fragment containing the *p63* promoter was cut from *p63:dsred* with XhoI and BamHI and cloned into the XhoI/BamHI site of p5E-MCS, which was then used in a Gateway LR reaction with pME-GFP-CAAX (Tol2 kit), p3E-polyA, and pDestTol2pA2. Final constructs were injected into 1–2–cell stage fertilized zebrafish embryos at a concentration of 12.5–25 ng/µl.

Morpholinos

MOs were obtained from Gene Tools and diluted in Danieau buffer before injection of 3 nl into fertilized eggs. Morpholino sequences and concentrations were as follows: MO1-spint1a (hai1a) 5′-ACCCTGAGTAGAGCCAGAGTCATCC-3′ (ZFIN: ZDB-MRPHLNO-071218-5), 20 µM (high) or 10 µM (low; Carney et al., 2007); par2b 5′-GTAGCTCTCGGACACCGCCATATTC-3′ (this paper), 500 µM; MO1-spi1b (pu.1) 5′-GATATACTGATACTCCAT TGGTGGT-3′ (ZDB-MRPHLNO-050224-1), 500 µM (Rhodes et al., 2005); MO1-st14a (mat1a) 5′-AACGCATTCCTCCATCCA TAGGGTC-3′ (ZDB-MRPHLNO-071218-1), 66.67 µM (Carney et al., 2007); MO3-lama5 5′-AACGCTTAGTTGGCACCTTGTTGG C-3′ (ZDB-MRPHLNO-080109-7), 50 µM (high) or 20 µM (low; Webb et al., 2007); and MO2-itga3b 5′-AGTCAAATGCGCTAA CTCACCCTGC-3′ (ZDB-MRPHLNO-100528-11), 50 µM (high) or 20 µM (low; Carney et al., 2010).

Inhibitors

All inhibitors were obtained from Sigma-Aldrich/Merck with the exception of MMP9 inhibitor I (Enzo) and MPA08 (Tocris). Stock solutions of drugs were prepared in DMSO, except for S1P, which was dissolved in methanol. Appropriate dilutions were prepared in E3 embryo medium before application to the embryos and were renewed each day of the treatment. Final concentrations were as follows: PD168393, 2.7 µM; FIPI, 100 µM; rapamycin, 1.1 µM; butanol, 0.3%; PIK-90, 5 µM; wortmannin, 1 µM; PD0325901, 1.5 µM; AICAR, 1.2 µM; MPA08, 50 µM (low)–100 µM (high); S1P, 0.2 µg/ml; MMP9 inhibitor I, 20 µM; MMP9/13 inhibitor, 50 µM; camptothecin, 20 nM; Rockout, 60 µM; blebbistatin, 5 µM; cytochalasin D, 2 µM; and ML141, 50 µM. Control embryos were incubated in vehicle (DMSO or methanol) at the same dilution as the drug-treated embryos.

Western blot

Protein extracts from tails of 48 hpf embryos prepared in lysis buffer supplemented with phosphatase and protease inhibitors (PhosSTOP, cOmplete protease inhibitor cocktail tablets, Roche) were separated by 9% SDS-PAGE under reducing conditions. Following transfer to a 0.2-µm nitrocellulose membrane (Amersham Protran), the membrane was blocked in 4% BSA in TBS-Tween. The primary antibody (rabbit polyclonal anti-phospho-S6 ribosomal protein Ser240/244, RRID AB_331682, Cell Signaling Technology, cat. no. 2215; mouse monoclonal anti-tubulin, RRID AB_477579, Sigma-Aldrich, cat. no. T5168; rabbit monoclonal anti-phospho-Akt Ser473, RRID AB_2315049, Cell Signaling Technology, cat. no. 4060; mouse monoclonal anti-MAP kinase, activated [diphosphorylated ERK1 and 2], RRID AB_260729, Sigma-Aldrich, cat. no. M9692) was diluted to 1:2,000 or 1:5,000 in blocking buffer and incubated with the membrane overnight at 4°C. The secondary antibody (goat anti-rabbit or anti-mouse HRP, RRID AB_2313567 or AB_10015289, Jackson ImmunoResearch, cat. no. 111-035-003 and 115-035-003) was diluted to 1:10,000, and the blot was developed using chemiluminescent substrate (Pierce ECL Western blotting substrate, Thermo Fisher Scientific). Relative protein levels were determined using Fiji/ImageJ software (Schindelin et al., 2012).

Downloaded from http://rupress.org/jcb/article-pdf/219/2/e201905190/1622245/jcb_201905190.pdf by guest on 05 December 2025

Fluorescent antibody and fluorescent dye staining

Embryos were fixed 2 h to overnight in 4% formaldehyde titrated from paraformaldehyde, washed extensively in PBS–Triton X-100 (0.5%), blocked in blocking buffer (4% fetal calf serum and 1% DMSO, in PBS–Triton X-100 0.5%), and incubated at 4°C with the primary antibody at the following dilutions: mouse monoclonal anti-P63, 1:500 (RRID AB_10588476, Biocare Medical, cat. no. CM163C); chicken polyclonal anti-GFP, 1:500 (RRID AB_2534023, Invitrogen, cat. no. A10262); mouse monoclonal anti-BrdU (RRID AB_514483, Roche, cat. no. 1170376001) or rabbit polyclonal anti-BrdU (Abcam, cat. no. 152095), 1:500; rabbit polyclonal anti-laminin, 1:500 (RRID AB_477163, Sigma-Aldrich, cat. no. L9393); and mouse monoclonal anti–E-cadherin, 1:200 (RRID AB_397581, BD Biosciences, cat. no. 610182). The following secondary antibodies were used, all diluted 1:1,000 in blocking buffer: goat anti-rabbit Alexa Fluor 488 (RRID AB_143165, cat. no. A11008), goat anti-chicken Alexa Fluor 488 (RRID AB_2534096, cat. no. A11039), goat anti-mouse Cy3 (RRID AB_2534030, cat. no. A10521), and goat anti-mouse Alexa Fluor 647 (RRID AB_2535804, cat. no. A21235; all Invitrogen).

For labeling f-actin, embryos were incubated for 15 min at room temperature with Phalloidin-TRITC (Sigma-Aldrich) or Phalloidin iFluor 647 (Abcam). To visualize nuclei, embryos were incubated for 15 min in DAPI (Sigma-Aldrich) diluted 1:1,000 in wash buffer, or live extruded cells were treated with DRAQ5 (Thermo Fisher Scientific) according to the manufacturer's instructions. For labeling of metabolically active mitochondria, MitoTracker Deep Red FM (Invitrogen) was applied according to the manufacturer's instructions. For visualization of lysosomes, LysoTracker Deep Red (Thermo Fisher Scientific) was diluted to 50 µM and applied to embryos or extruded cells for 30 min before imaging, as described by the manufacturer. Acridine Orange (Sigma-Aldrich) was diluted to 0.01 mg/ml in E3 embryo medium and applied to live embryos for 30 min, followed by washing with E3 embryo medium. Embryos were anesthetized with MESAB and imaged live. Embryos exposed to UV for 10 s, followed by 6 h of recovery time, served as a positive control for apoptosis. Staining with Sytox AADvanced Dead Cell Stain Kit (Thermo Fisher Scientific) was performed according to the manufacturer's instructions. Exposure to topoisomerase inhibitor 20 nM camptothecin (Sigma-Aldrich) for 6 h before imaging served as a positive control. TUNEL assay (In Situ Cell Death Detection Kit, Roche) was performed on PFA-fixed embryos following the manufacturer's instructions. Embryos treated with 300 U/ml DNaseI for 10 min before the TUNEL reaction served as a positive control, while embryos incubated in label mixture without enzyme served as a negative control.

Images were obtained with a Zeiss LSM 710 or LSM 700 confocal microscope and processed using Fiji software.

Avidin/biotin complex (ABC)/DAB colorimetric antibody staining

For visualization of skin cells with phosphorylated EGFR, embryos were fixed overnight at 4°C in ethanol–acetic acid–formaldehyde fixative (40% ethanol, 5% acetic acid, and 10% formalin), and washed extensively in 0.1% PBS–Tween-20. Quenching of endogenous peroxidases was achieved by incubating the embryos in 3% H_2O_2 for 5 min. Blocking was performed in blocking buffer (2% BSA, 1% DMSO, in 0.1% PBS–Tween-20) for at least 2 h, and embryos were incubated in primary antibody (polyclonal anti-pEGFR [Tyr1068], RRID AB_2533754, Thermo Fisher Scientific, cat. no. 44-788G) at a 1:50 dilution overnight at 4°C, and then with a biotinylated goat anti-rabbit secondary at 1:250 (RRID AB_2313606, Vector Laboratories, cat. no. BA-1000) following extensive washing. ABC amplification was performed following the manufacturer's instructions (Vectastain Elite ABC Peroxidase kit, Vector Labs), and embryos were incubated in DAB substrate (Sigma-Aldrich) and H_2O_2 until development of a signal. Embryos were then post-fixed in 4% PFA, transferred to methanol, and cleared in benzyl alcohol/benzyl benzoate (1:2; both Sigma-Aldrich) before imaging using a Zeiss Axioplan 2 microscope.

Counting of apically extruded cells

In general, zebrafish embryos were manually dechorionated at 24 hpf and placed in 24-well plates in E3 embryo medium containing inhibitors or the appropriately diluted vehicle. Following overnight (16 h) incubation, E3 embryo medium containing extruded cells was collected, and the wells were washed once with E3 embryo medium and collected. The recovered cells were pelleted in a hanging bucket centrifuge (Hereaus Multifuge X3R) by centrifugation at 500 × *g* for 5 min, and the supernatant was removed. The number of cells was counted using a hemocytometer (Neubauer Improved, Marienfeld), and the total number of cells per fish over the incubation period of 16 h was calculated. To distinguish dead from live extruded cells, collected cells were stained with 0.4% trypan blue (Invitrogen) before counting. For imaging and counting of GFP-positive peridermal cells and dsRed-positive basal keratinocytes, cells were collected as above, mounted on a coverslip, and imaged using a Zeiss LSM 700 confocal microscope.

In situ hybridization (*mmp9* probe)

mmp9 in situ hybridization was performed as previously described (Reischauer et al., 2009). Briefly, the following primers were used to PCR-amplify *mmp9* from 48 hpf embryo cDNA, the product of which was subsequently cloned into pGEM-T Easy Vector (Promega): forward 5′-GCTGCTCATGAG TTTGGAC-3′; reverse 5′-CCGAGCTTCTCGATTTTACG-3′. This *mmp9* template was linearized with *Nco*I (New England Biolabs), and digoxigenin-labeled antisense probe was synthesized using the Roche digoxygenin RNA synthesis kit and Sp6 RNA polymerase. The hybridization step occurred at 65°C. Embryos were transferred to benzyl benzoate/benzyl alcohol (2:1) and stored at 4°C until imaging.

Quantitative-RT-PCR (Q-RT-PCR)

Total RNA was isolated from amputated tails of zebrafish embryos at 48 and 96 hpf using Trizol (Thermo Fisher Scientific) following the manufacturer's instructions, and treated with DNaseI (Roche). First-strand cDNA synthesis was performed using reverse transcription (Promega). Q-RT-PCR was performed in triplicate with Sybr Select Master Mix (Life Technologies, Thermo Fisher Scientific) on an ABI-Prism 7500 Fast

Downloaded from http://rupress.org/jcb/article-pdf/219/2/e201905190/1622245/jcb_201905190.pdf by guest on 05 December 2025

Detect system, and relative expression levels were calculated following the $^{\Delta\Delta}$Ct method with *gapdh* as the control gene. Data are presented as fold change relative to the relevant sibling control and represent the average of at least three independent experiments unless otherwise indicated. Primer sequences were as follows: *gapdh* forward 5′-CGCTGGCATCTCCCTCAA-3′, *gapdh* reverse 5′-TCAGCAACACGATGGCTGTAG-3′ (Tang et al., 2007), *mmp9* forward 5′-TGATGTGCTTGGACCACGTAA-3′, *mmp9* reverse 5′-ACAGGAGCACCTTGCCTTTTC-3′ (Freisinger and Huttenlocher, 2014), *hai1a* forward 5′-GGAGCACAGAGAAGATCCTA-3′, and *hai1a* reverse 5′-CGTGGAGGTCTATCCTCTACA T-3′ (this paper; primers were designed using sequence NM_213152.1).

Hai1a sequencing

Sanger sequencing of the *hai1a* gene was performed by GATC (Eurofins) using the following primers: Sequencing primer *hai1a* forward 5′-ATGTAGAGGATAGACCTCCACG-3′, and sequencing primer *hai1a* reverse 5′-TACTGGTCACCCACCCTCAT-3′ (this paper).

Microscope image acquisition

All images were acquired at room temperature. Bright field images of live embryos mounted in 3% methyl cellulose/1× tricaine (Sigma-Aldrich) in embryo medium were acquired using a Leica M165FC stereo microscope with DFC425C camera and Leica Application Suite V3.8 software. Images of DAB-stained embryos mounted in benzyl alcohol/benzyl benzoate were obtained with a Zeiss Axiophot microscope, 20× Plan-Neofluar objective, AxioCam HRc camera, and Axiovision software. Confocal images of embryos mounted in low-melting-point agarose in E3 embryo medium were obtained using a Zeiss LSM 710 or LSM 700 confocal microscope, 40×/1.1 W Korr LD C-Apochromat, or 20×/0.8 Plan-Apochromat objective and Zen 2.3 SP1 software. Images were processed using Fiji/ImageJ software, including generation of orthogonal projections, maximum intensity projections, and adjustment of brightness and contrast.

Quantification and statistical analysis

Results are presented in figures as the mean, with error bars indicating SD. Unless otherwise indicated, data are from at least three independent experiments, and *n* indicated in figure legends represents the number of embryos or cells per condition. Statistical analysis was performed using GraphPad Prism software, with statistical significance determined as $P < 0.05$. For comparison of multiple groups, one-way ANOVA with posthoc Tukey's test was used to determine significance. Different letters above a graph indicate a statistically significant difference; for results of individual post hoc Tukey's multiple comparison tests, please refer to Table S1. For Q-RT-PCR experiments, mutants were compared with their relevant sibling control using an unpaired, two-tailed Student's *t* test.

Online supplemental material

Fig. S1 shows bright-field images of the lethal *hai1a*^{fr26} phenotype between 24 and 96 hpf, and shows that the *hai1a*^{fr26} phenotype is not dependent on inflammation, by impairing formation of the myeloid cell lineage using the *pu.1* MO. Fig. S2 shows Western blots and bright field images indicating that PI3K/Akt, MEK/ERK, and Ampk do not contribute to the *hai1a* skin phenotype; and representative confocal images and resultant plot profiles indicating how EGFP-PASS ratios were calculated. Fig. S3 shows that cell death does not occur on the surface of the epidermis in *hai1a*^{hi2217} mutants, using TUNEL, Acridine Orange, and Sytox staining as different indicators of cell death; cell extrusion counts in the presence of trypan blue to distinguish live from dead cells; and DRAQ5 and mitoTracker staining of recovered extruded cells indicating that the cells are alive and metabolically active. Fig. S4 shows representative bright field images of embryos treated with the sphingosine kinase inhibitor MPA08; a mitogenic effect of exogenous S1P only when applied for 4 d; and the absence of an effect of exogenous S1P on cell–matrix or cell–cell adhesions. Fig. S5 shows alternative rapamycin/S1P drug treatment regimes, which do not improve long-term survival despite alleviating proliferation. Video 1 shows a confocal z-stack of cell extrusion on the surface of a zebrafish embryo. Video 2 shows a confocal z-stack of a cluster of extruded cells recovered from the embryo growth medium. Table S1 lists the results of each Tukey's multiple comparison test following one-way ANOVA.

Acknowledgments

The authors wish to thank Sandra Rieger, Guangwei Du, Nicholas Ktistakis, and Anna Huttenlocher for providing vital reagents.

Work in the laboratory of M. Hammerschmidt was supported by the Deutsche Forschungsgemeinschaft (SFB 829 and its Z2 project), the National Institute of General Medical Sciences (GM63904), and the Center for Molecular Medicine Cologne, University of Cologne.

The authors declare no competing financial interests.

Author contributions: Conceptualization and Methodology: J. Armistead, J. Hatzold, and M. Hammerschmidt; Formal Analysis: J. Armistead and A. van Roye; Investigation: J. Armistead, J. Hatzold, A. van Roye, and E. Fahle; Writing of Manuscript: J. Armistead and M. Hammerschmidt; Supervision and Project Administration: M. Hammerschmidt; and Funding Acquisition, M. Hammerschmidt and J. Armistead.

Submitted: 24 May 2019
Revised: 2 October 2019
Accepted: 4 November 2019

References

Amsterdam, A., R.M. Nissen, Z. Sun, E.C. Swindell, S. Farrington, and N. Hopkins. 2004. Identification of 315 genes essential for early zebrafish development. *Proc. Natl. Acad. Sci. USA.* 101:12792–12797. https://doi.org/10.1073/pnas.0403929101

Anastasaki, C., K.A. Rauen, and E.E. Patton. 2012. Continual low-level MEK inhibition ameliorates cardio-facio-cutaneous phenotypes in zebrafish. *Dis. Model. Mech.* 5:546–552. https://doi.org/10.1242/dmm.008672

Anton, K.A., M. Kajita, R. Narumi, Y. Fujita, and M. Tada. 2018. Src-transformed cells hijack mitosis to extrude from the epithelium. *Nat. Commun.* 9:4695. https://doi.org/10.1038/s41467-018-07163-4

Downloaded from http://rupress.org/jcb/article-pdf/219/2/e201905190/1622245/jcb_201905190.pdf by guest on 05 December 2025

Arasada, R.R., J.M. Amann, M.A. Rahman, S.S. Huppert, and D.P. Carbone. 2014. EGFR blockade enriches for lung cancer stem-like cells through Notch3-dependent signaling. *Cancer Res.* 74:5572–5584. https://doi.org/10.1158/0008-5472.CAN-13-3724

Ávalos, Y., J. Canales, R. Bravo-Sagua, A. Criollo, S. Lavandero, and A.F. Quest. 2014. Tumor suppression and promotion by autophagy. *BioMed Res. Int.* 2014:603980. https://doi.org/10.1155/2014/603980

Ballou, L.M., Y.P. Jiang, G. Du, M.A. Frohman, and R.Z. Lin. 2003. Ca(2+)- and phospholipase D-dependent and -independent pathways activate mTOR signaling. *FEBS Lett.* 550:51–56. https://doi.org/10.1016/S0014-5793(03)00816-0

Bernut, A., J.L. Herrmann, K. Kissa, J.F. Dubremetz, J.L. Gaillard, G. Lutfalla, and L. Kremer. 2014. Mycobacterium abscessus cording prevents phagocytosis and promotes abscess formation. *Proc. Natl. Acad. Sci. USA.* 111:E943–E952. https://doi.org/10.1073/pnas.1321390111

Bohdanowicz, M., D. Schlam, M. Hermansson, D. Rizzuti, G.D. Fairn, T. Ueyama, P. Somerharju, G. Du, and S. Grinstein. 2013. Phosphatidic acid is required for the constitutive ruffling and macropinocytosis of phagocytes. *Mol. Biol. Cell.* 24:1700–1712: S1–S7. https://doi.org/10.1091/mbc.e12-11-0789

Bruntz, R.C., C.W. Lindsley, and H.A. Brown. 2014. Phospholipase D signaling pathways and phosphatidic acid as therapeutic targets in cancer. *Pharmacol. Rev.* 66:1033–1079. https://doi.org/10.1124/pr.114.009217

Carney, T.J., S. von der Hardt, C. Sonntag, A. Amsterdam, J. Topczewski, N. Hopkins, and M. Hammerschmidt. 2007. Inactivation of serine protease Matriptase1a by its inhibitor Hai1 is required for epithelial integrity of the zebrafish epidermis. *Development.* 134:3461–3471. https://doi.org/10.1242/dev.004556

Carney, T.J., N.M. Feitosa, C. Sonntag, K. Slanchev, J. Kluger, D. Kiyozumi, J.M. Gebauer, J. Coffin Talbot, C.B. Kimmel, K. Sekiguchi, et al. 2010. Genetic analysis of fin development in zebrafish identifies furin and hemicentin1 as potential novel fraser syndrome disease genes. *PLoS Genet.* 6:e1000907. https://doi.org/10.1371/journal.pgen.1000907

Chen, M., L.-M. Chen, C.-Y. Lin, and K.X. Chai. 2008. The epidermal growth factor receptor (EGFR) is proteolytically modified by the Matriptase-Prostasin serine protease cascade in cultured epithelial cells. *Biochim. Biophys. Acta.* 1783:896–903. https://doi.org/10.1016/j.bbamcr.2007.10.019

Choo, A.Y., S.O. Yoon, S.G. Kim, P.P. Roux, and J. Blenis. 2008. Rapamycin differentially inhibits S6Ks and 4E-BP1 to mediate cell-type-specific repression of mRNA translation. *Proc. Natl. Acad. Sci. USA.* 105:17414–17419. https://doi.org/10.1073/pnas.0809136105

Cserzö, M., F. Eisenhaber, B. Eisenhaber, and I. Simon. 2002. On filtering false positive transmembrane protein predictions. *Protein Eng.* 15:745–752. https://doi.org/10.1093/protein/15.9.745

Dall'Armi, C., A. Hurtado-Lorenzo, H. Tian, E. Morel, A. Nezu, R.B. Chan, W.H. Yu, K.S. Robinson, O. Yeku, S.A. Small, et al. 2010. The phospholipase D1 pathway modulates macroautophagy. *Nat. Commun.* 1:142. https://doi.org/10.1038/ncomms1144

Dany, M. 2017. Sphingosine metabolism as a therapeutic target in cutaneous melanoma. *Transl. Res.* 185:1–12. https://doi.org/10.1016/j.trsl.2017.04.005

Davis, N.M., M. Sokolosky, K. Stadelman, S.L. Abrams, M. Libra, S. Candido, F. Nicoletti, J. Polesel, R. Maestro, A. D'Assoro, et al. 2014. Deregulation of the EGFR/PI3K/PTEN/Akt/mTORC1 pathway in breast cancer: possibilities for therapeutic intervention. *Oncotarget.* 5:4603–4650. https://doi.org/10.18632/oncotarget.2209

Delon, C., M. Manifava, E. Wood, D. Thompson, S. Krugmann, S. Pyne, and N.T. Ktistakis. 2004. Sphingosine kinase 1 is an intracellular effector of phosphatidic acid. *J. Biol. Chem.* 279:44763–44774. https://doi.org/10.1074/jbc.M405771200

Durgan, J., Y.-Y. Tseng, J.C. Hamann, M.-C. Domart, L. Collinson, A. Hall, M. Overholtzer, and O. Florey. 2017. Mitosis can drive cell cannibalism through entosis. *eLife.* 6:e27134. https://doi.org/10.7554/eLife.27134

Eisenhoffer, G.T., P.D. Loftus, M. Yoshigi, H. Otsuna, C.B. Chien, P.A. Morcos, and J. Rosenblatt. 2012. Crowding induces live cell extrusion to maintain homeostatic cell numbers in epithelia. *Nature.* 484:546–549. https://doi.org/10.1038/nature10999

Ellis, S.J., N.C. Gomez, J. Levorse, A.F. Mertz, Y. Ge, and E. Fuchs. 2019. Distinct modes of cell competition shape mammalian tissue morphogenesis. *Nature.* 569:497–502. https://doi.org/10.1038/s41586-019-1199-y

Fang, Y., M. Vilella-Bach, R. Bachmann, A. Flanigan, and J. Chen. 2001. Phosphatidic acid-mediated mitogenic activation of mTOR signaling. *Science.* 294:1942–1945. https://doi.org/10.1126/science.1066015

Florey, O., S.E. Kim, C.P. Sandoval, C.M. Haynes, and M. Overholtzer. 2011. Autophagy machinery mediates macroendocytic processing and entotic cell death by targeting single membranes. *Nat. Cell Biol.* 13:1335–1343. https://doi.org/10.1038/ncb2363

Freisinger, C.M., and A. Huttenlocher. 2014. Live imaging and gene expression analysis in zebrafish identifies a link between neutrophils and epithelial to mesenchymal transition. *PLoS One.* 9:e112183. https://doi.org/10.1371/journal.pone.0112183

Giannelli, G., J. Falk-Marzillier, O. Schiraldi, W.G. Stetler-Stevenson, and V. Quaranta. 1997. Induction of cell migration by matrix metalloprotease-2 cleavage of laminin-5. *Science.* 277:225–228. https://doi.org/10.1126/science.277.5323.225

Gong, Z., B. Ju, X. Wang, J. He, H. Wan, P.M. Sudha, and T. Yan. 2002. Green fluorescent protein expression in germ-line transmitted transgenic zebrafish under a stratified epithelial promoter from keratin8. *Dev. Dyn.* 223:204–215. https://doi.org/10.1002/dvdy.10051

Grieve, A.G., and C. Rabouille. 2014. Extracellular cleavage of E-cadherin promotes epithelial cell extrusion. *J. Cell Sci.* 127:3331–3346. https://doi.org/10.1242/jcs.147926

Gu, Y., T. Forostyan, R. Sabbadini, and J. Rosenblatt. 2011. Epithelial cell extrusion requires the sphingosine-1-phosphate receptor 2 pathway. *J. Cell Biol.* 193:667–676. https://doi.org/10.1083/jcb.201010075

Gu, Y., J. Shea, G. Slattum, M.A. Firpo, M. Alexander, S.J. Mulvihill, V.M. Golubovskaya, and J. Rosenblatt. 2015. Defective apical extrusion signaling contributes to aggressive tumor hallmarks. *eLife.* 4:e04069. https://doi.org/10.7554/eLife.04069

Gude, D.R., S.E. Alvarez, S.W. Paugh, P. Mitra, J. Yu, R. Griffiths, S.E. Barbour, S. Milstien, and S. Spiegel. 2008. Apoptosis induces expression of sphingosine kinase 1 to release sphingosine-1-phosphate as a "come-and-get-me" signal. *FASEB J.* 22:2629–2638. https://doi.org/10.1096/fj.08-107169

Hatzold, J., F. Beleggia, H. Herzig, J. Altmüller, P. Nürnberg, W. Bloch, B. Wollnik, and M. Hammerschmidt. 2016. Tumor suppression in basal keratinocytes via dual non-cell-autonomous functions of a Na,K-ATPase beta subunit. *eLife.* 5:e14277. https://doi.org/10.7554/eLife.14277

Henkels, K.M., G.P. Boivin, E.S. Dudley, S.J. Berberich, and J. Gomez-Cambronero. 2013. Phospholipase D (PLD) drives cell invasion, tumor growth and metastasis in a human breast cancer xenograph model. *Oncogene.* 32:5551–5562. https://doi.org/10.1038/onc.2013.207

Holcmann, M., and M. Sibilia. 2015. Mechanisms underlying skin disorders induced by EGFR inhibitors. *Mol. Cell. Oncol.* 2:e1004969. https://doi.org/10.1080/23723556.2015.1004969

Huang, L., and L. Fu. 2015. Mechanisms of resistance to EGFR tyrosine kinase inhibitors. *Acta Pharm. Sin. B.* 5:390–401. https://doi.org/10.1016/j.apsb.2015.07.001

Krajcovic, M., N.B. Johnson, Q. Sun, G. Normand, N. Hoover, E. Yao, A.L. Richardson, R.W. King, E.S. Cibas, S.J. Schnitt, et al. 2011. A non-genetic route to aneuploidy in human cancers. *Nat. Cell Biol.* 13:324–330. https://doi.org/10.1038/ncb2174

Krishna, S., and M. Overholtzer. 2016. Mechanisms and consequences of entosis. *Cell. Mol. Life Sci.* 73:2379–2386. https://doi.org/10.1007/s00018-016-2207-0

Kunkel, G.T., M. Maceyka, S. Milstien, and S. Spiegel. 2013. Targeting the sphingosine-1-phosphate axis in cancer, inflammation and beyond. *Nat. Rev. Drug Discov.* 12:688–702. https://doi.org/10.1038/nrd4099

Kupperman, E., S. An, N. Osborne, S. Waldron, and D.Y. Stainier. 2000. A sphingosine-1-phosphate receptor regulates cell migration during vertebrate heart development. *Nature.* 406:192–195. https://doi.org/10.1038/35018092

Kwan, K.M., E. Fujimoto, C. Grabher, B.D. Mangum, M.E. Hardy, D.S. Campbell, J.M. Parant, H.J. Yost, J.P. Kanki, and C.B. Chien. 2007. The Tol2kit: a multisite gateway-based construction kit for Tol2 transposon transgenesis constructs. *Dev. Dyn.* 236:3088–3099. https://doi.org/10.1002/dvdy.21343

LeBert, D.C., J.M. Squirrell, J. Rindy, E. Broadbridge, Y. Lui, A. Zakrzewska, K.W. Eliceiri, A.H. Meijer, and A. Huttenlocher. 2015. Matrix metalloproteinase 9 modulates collagen matrices and wound repair. *Development.* 142:2136–2146. https://doi.org/10.1242/dev.121160

Lebrun, J.-J. 2012. The Dual Role of TGFβ in Human Cancer: From Tumor Suppression to Cancer Metastasis. *ISRN Mol. Biol.* 2012:381428.

Lee, S.L., R.B. Dickson, and C.Y. Lin. 2000. Activation of hepatocyte growth factor and urokinase/plasminogen activator by matriptase, an epithelial membrane serine protease. *J. Biol. Chem.* 275:36720–36725. https://doi.org/10.1074/jbc.M007802200

Downloaded from http://rupress.org/jcb/article-pdf/219/2/e201905190/1622245/jcb_201905190.pdf by guest on 05 December 2025

Lee, R.T.H., P.V. Asharani, and T.J. Carney. 2014. Basal keratinocytes contribute to all strata of the adult zebrafish epidermis. *PLoS One.* 9:e84858. https://doi.org/10.1371/journal.pone.0084858

Lee, Y., J.C. Hamann, M. Pellegrino, J. Durgan, M.C. Domart, L.M. Collinson, C.M. Haynes, O. Florey, and M. Overholtzer. 2019. Entosis Controls a Developmental Cell Clearance in C. elegans. *Cell Reports.* 26: 3212–3220.e4. https://doi.org/10.1016/j.celrep.2019.02.073

Lisse, T.S., L.J. Middleton, A.D. Pellegrini, P.B. Martin, E.L. Spaulding, O. Lopes, E.A. Brochu, E.V. Carter, A. Waldron, and S. Rieger. 2016. Paclitaxel-induced epithelial damage and ectopic MMP-13 expression promotes neurotoxicity in zebrafish. *Proc. Natl. Acad. Sci. USA.* 113: E2189–E2198. https://doi.org/10.1073/pnas.1525096113

List, K., T.H. Bugge, and R. Szabo. 2006. Matriptase: potent proteolysis on the cell surface. *Mol. Med.* 12:1–7. https://doi.org/10.2119/2006-00022.List

List, K., P. Kosa, R. Szabo, A.L. Bey, C.B. Wang, A. Molinolo, and T.H. Bugge. 2009. Epithelial integrity is maintained by a matriptase-dependent proteolytic pathway. *Am. J. Pathol.* 175:1453–1463. https://doi.org/10.2353/ajpath.2009.090240

Loizou, E., A. Banito, G. Livshits, Y.J. Ho, R.P. Koche, F.J. Sánchez-Rivera, A. Mayle, C.C. Chen, S. Kinalis, F.O. Bagger, et al. 2019. A Gain-of-Function p53-Mutant Oncogene Promotes Cell Fate Plasticity and Myeloid Leukemia through the Pluripotency Factor FOXH1. *Cancer Discov.* 9: 962–979. https://doi.org/10.1158/2159-8290.CD-18-1391

Marchler-Bauer, A., Y. Bo, L. Han, J. He, C.J. Lanczycki, S. Lu, F. Chitsaz, M.K. Derbyshire, R.C. Geer, N.R. Gonzales, et al. 2017. CDD/SPARCLE: functional classification of proteins via subfamily domain architectures. *Nucleic Acids Res.* 45(D1):D200–D203. https://doi.org/10.1093/nar/gkw1129

Marinari, E., A. Mehonic, S. Curran, J. Gale, T. Duke, and B. Baum. 2012. Live-cell delamination counterbalances epithelial growth to limit tissue overcrowding. *Nature.* 484:542–545. https://doi.org/10.1038/nature10984

Martin, L.A., F. André, M. Campone, T. Bachelot, and G. Jerusalem. 2013. mTOR inhibitors in advanced breast cancer: ready for prime time? *Cancer Treat. Rev.* 39:742–752. https://doi.org/10.1016/j.ctrv.2013.02.005

Martins, I., S.Q. Raza, L. Voisin, H. Dakhli, F. Law, D. De Jong, A. Allouch, M. Thoreau, C. Brenner, E. Deutsch, and J.L. Perfettini. 2017. Entosis: The emerging face of non-cell-autonomous type IV programmed death. *Biomed. J.* 40:133–140. https://doi.org/10.1016/j.bj.2017.05.001

Mathias, J.R., M.E. Dodd, K.B. Walters, J. Rhodes, J.P. Kanki, A.T. Look, and A. Huttenlocher. 2007. Live imaging of chronic inflammation caused by mutation of zebrafish Hai1. *J. Cell Sci.* 120:3372–3383. https://doi.org/10.1242/jcs.009159

Monks, J., D. Rosner, F.J. Geske, L. Lehman, L. Hanson, M.C. Neville, and V.A. Fadok. 2005. Epithelial cells as phagocytes: apoptotic epithelial cells are engulfed by mammary alveolar epithelial cells and repress inflammatory mediator release. *Cell Death Differ.* 12:107–114. https://doi.org/10.1038/sj.cdd.4401517

Monks, J., C. Smith-Steinhart, E.R. Kruk, V.A. Fadok, and P.M. Henson. 2008. Epithelial cells remove apoptotic epithelial cells during post-lactation involution of the mouse mammary gland. *Biol. Reprod.* 78:586–594. https://doi.org/10.1095/biolreprod.107.065045

Oberst, M.D., M.D. Johnson, R.B. Dickson, C.-Y. Lin, B. Singh, M. Stewart, A. Williams, A. al-Nafussi, J.F. Smyth, H. Gabra, and G.C. Sellar. 2002. Expression of the serine protease matriptase and its inhibitor HAI-1 in epithelial ovarian cancer: correlation with clinical outcome and tumor clinicopathological parameters. *Clin. Cancer Res.* 8:1101–1107.

Overholtzer, M., A.A. Mailleux, G. Mouneimne, G. Normand, S.J. Schnitt, R.W. King, E.S. Cibas, and J.S. Brugge. 2007. A nonapoptotic cell death process, entosis, that occurs by cell-in-cell invasion. *Cell.* 131:966–979. https://doi.org/10.1016/j.cell.2007.10.040

Park, J.B., C.S. Lee, J.-H. Jang, J. Ghim, Y.-J. Kim, S. You, D. Hwang, P.-G. Suh, and S.H. Ryu. 2012. Phospholipase signalling networks in cancer. *Nat. Rev. Cancer.* 12:782–792. https://doi.org/10.1038/nrc3379

Purvanov, V., M. Holst, J. Khan, C. Baarlink, and R. Grosse. 2014. G-protein-coupled receptor signaling and polarized actin dynamics drive cell-in-cell invasion. *eLife.* 3:e02786. https://doi.org/10.7554/eLife.02786

Pyne, S., R. Bittman, and N.J. Pyne. 2011. Sphingosine kinase inhibitors and cancer: seeking the golden sword of Hercules. *Cancer Res.* 71:6576–6582. https://doi.org/10.1158/0008-5472.CAN-11-2364

Rada, M., N. Barlev, and S. Macip. 2018. BTK: a two-faced effector in cancer and tumour suppression. *Cell Death Dis.* 9:1064. https://doi.org/10.1038/s41419-018-1122-8

Reischauer, S., M.P. Levesque, C. Nüsslein-Volhard, and M. Sonawane. 2009. Lgl2 executes its function as a tumor suppressor by regulating ErbB signaling in the zebrafish epidermis. *PLoS Genet.* 5:e1000720. https://doi.org/10.1371/journal.pgen.1000720

Renshaw, S.A., C.A. Loynes, D.M. Trushell, S. Elworthy, P.W. Ingham, and M.K. Whyte. 2006. A transgenic zebrafish model of neutrophilic inflammation. *Blood.* 108:3976–3978. https://doi.org/10.1182/blood-2006-05-024075

Rhodes, J., A. Hagen, K. Hsu, M. Deng, T.X. Liu, A.T. Look, and J.P. Kanki. 2005. Interplay of pu.1 and gata1 determines myelo-erythroid progenitor cell fate in zebrafish. *Dev. Cell.* 8:97–108. https://doi.org/10.1016/j.devcel.2004.11.014

Rosenblatt, J., M.C. Raff, and L.P. Cramer. 2001. An epithelial cell destined for apoptosis signals its neighbors to extrude it by an actin- and myosin-dependent mechanism. *Curr. Biol.* 11:1847–1857. https://doi.org/10.1016/S0960-9822(01)00587-5

Saxton, R.A., and D.M. Sabatini. 2017. mTOR Signaling in Growth, Metabolism, and Disease. *Cell.* 168:960–976. https://doi.org/10.1016/j.cell.2017.02.004

Schepis, A., A. Barker, Y. Srinivasan, E. Balouch, Y. Zheng, I. Lam, H. Clay, C.D. Hsiao, and S.R. Coughlin. 2018. Protease signaling regulates apical cell extrusion, cell contacts, and proliferation in epithelia. *J. Cell Biol.* 217:1097–1112. https://doi.org/10.1083/jcb.201709118

Schindelin, J., I. Arganda-Carreras, E. Frise, V. Kaynig, M. Longair, T. Pietzsch, S. Preibisch, C. Rueden, S. Saalfeld, B. Schmid, et al. 2012. Fiji: an open-source platform for biological-image analysis. *Nat. Methods.* 9: 676–682. https://doi.org/10.1038/nmeth.2019

Scott, S.A., P.E. Selvy, J.R. Buck, H.P. Cho, T.L. Criswell, A.L. Thomas, M.D. Armstrong, C.L. Arteaga, C.W. Lindsley, and H.A. Brown. 2009. Design of isoform-selective phospholipase D inhibitors that modulate cancer cell invasiveness. *Nat. Chem. Biol.* 5:108–117. https://doi.org/10.1038/nchembio.140

Siddhanta, A., J.M. Backer, and D. Shields. 2000. Inhibition of phosphatidic acid synthesis alters the structure of the Golgi apparatus and inhibits secretion in endocrine cells. *J. Biol. Chem.* 275:12023–12031. https://doi.org/10.1074/jbc.275.16.12023

Slaaby, R., T. Jensen, H.S. Hansen, M.A. Frohman, and K. Seedorf. 1998. PLD2 complexes with the EGF receptor and undergoes tyrosine phosphorylation at a single site upon agonist stimulation. *J. Biol. Chem.* 273: 33722–33727. https://doi.org/10.1074/jbc.273.50.33722

Slattum, G., K.M. McGee, and J. Rosenblatt. 2009. P115 RhoGEF and microtubules decide the direction apoptotic cells extrude from an epithelium. *J. Cell Biol.* 186:693–702. https://doi.org/10.1083/jcb.200903079

Sonawane, M., Y. Carpio, R. Geisler, H. Schwarz, H.-M. Maischein, and C. Nuesslein-Volhard. 2005. Zebrafish penner/lethal giant larvae 2 functions in hemidesmosome formation, maintenance of cellular morphology and growth regulation in the developing basal epidermis. *Development.* 132:3255–3265. https://doi.org/10.1242/dev.01904

Su, W., O. Yeku, S. Olepu, A. Genna, J.S. Park, H. Ren, G. Du, M.H. Gelb, A.J. Morris, and M.A. Frohman. 2009. 5-Fluoro-2-indolyl des-chlorohalopemide (FIPI), a phospholipase D pharmacological inhibitor that alters cell spreading and inhibits chemotaxis. *Mol. Pharmacol.* 75: 437–446. https://doi.org/10.1124/mol.108.053298

Szabo, R., and T.H. Bugge. 2011. Membrane-anchored serine proteases in vertebrate cell and developmental biology. *Annu. Rev. Cell Dev. Biol.* 27: 213–235. https://doi.org/10.1146/annurev-cellbio-092910-154247

Szabo, R., A.L. Rasmussen, A.B. Moyer, P. Kosa, J.M. Schafer, A.A. Molinolo, J.S. Gutkind, and T.H. Bugge. 2011. c-Met-induced epithelial carcinogenesis is initiated by the serine protease matriptase. *Oncogene.* 30: 2003–2016. https://doi.org/10.1038/onc.2010.586

Tang, R., A. Dodd, D. Lai, W.C. McNabb, and D.R. Love. 2007. Validation of zebrafish (Danio rerio) reference genes for quantitative real-time RT-PCR normalization. *Acta Biochim. Biophys. Sin. (Shanghai).* 39:384–390. https://doi.org/10.1111/j.1745-7270.2007.00283.x

Tripathi, M., A.A. Potdar, H. Yamashita, B. Weidow, P.T. Cummings, D. Kirchhofer, and V. Quaranta. 2011. Laminin-332 cleavage by matriptase alters motility parameters of prostate cancer cells. *Prostate.* 71:184–196. https://doi.org/10.1002/pros.21233

Tsaur, I., J. Makarević, E. Juengel, M. Gasser, A.M. Waaga-Gasser, M. Kurosch, M. Reiter, S. Wedel, G. Bartsch, A. Haferkamp, et al. 2012. Resistance to the mTOR-inhibitor RAD001 elevates integrin α2- and β1-triggered motility, migration and invasion of prostate cancer cells. *Br. J. Cancer.* 107:847–855. https://doi.org/10.1038/bjc.2012.313

Downloaded from http://rupress.org/jcb/article-pdf/219/2/e201905190/1622245/jcb_201905190.pdf by guest on 05 December 2025

Turunen, S.P., O. Tatti-Bugaeva, and K. Lehti. 2017. Membrane-type matrix metalloproteases as diverse effectors of cancer progression. *Biochim. Biophys. Acta Mol. Cell. Res.* 1864:1974–1988. https://doi.org/10.1016/j.bbamcr.2017.04.002

Urasaki, A., G. Morvan, and K. Kawakami. 2006. Functional dissection of the Tol2 transposable element identified the minimal cis-sequence and a highly repetitive sequence in the subterminal region essential for transposition. *Genetics.* 174:639–649. https://doi.org/10.1534/genetics.106.060244

Webb, A.E., J. Sanderford, D. Frank, W.S. Talbot, W. Driever, and D. Kimelman. 2007. Laminin α5 is essential for the formation of the zebrafish fins. *Dev. Biol.* 311:369–382. https://doi.org/10.1016/j.ydbio.2007.08.034

Wiley, D.S., S.E. Redfield, and L.I. Zon. 2017. Chemical screening in zebrafish for novel biological and therapeutic discovery. *Methods Cell Biol.* 138:651–679. https://doi.org/10.1016/bs.mcb.2016.10.004

Ye, J., M. Kawaguchi, Y. Haruyama, A. Kanemaru, T. Fukushima, K. Yamamoto, C.Y. Lin, and H. Kataoka. 2014. Loss of hepatocyte growth factor activator inhibitor type 1 participates in metastatic spreading of human pancreatic cancer cells in a mouse orthotopic transplantation model. *Cancer Sci.* 105:44–51. https://doi.org/10.1111/cas.12306

Yoo, S.K., Q. Deng, P.J. Cavnar, Y.I. Wu, K.M. Hahn, and A. Huttenlocher. 2010. Differential regulation of protrusion and polarity by PI3K during neutrophil motility in live zebrafish. *Dev. Cell.* 18:226–236. https://doi.org/10.1016/j.devcel.2009.11.015

Zandi, R., A.B. Larsen, P. Andersen, M.T. Stockhausen, and H.S. Poulsen. 2007. Mechanisms for oncogenic activation of the epidermal growth factor receptor. *Cell. Signal.* 19:2013–2023. https://doi.org/10.1016/j.cellsig.2007.06.023

Zhang, H., N.N. Desai, A. Olivera, T. Seki, G. Brooker, and S. Spiegel. 1991. Sphingosine-1-phosphate, a novel lipid, involved in cellular proliferation. *J. Cell Biol.* 114:155–167. https://doi.org/10.1083/jcb.114.1.155

Zhang, F., Z. Wang, M. Lu, Y. Yonekubo, X. Liang, Y. Zhang, P. Wu, Y. Zhou, S. Grinstein, J.F. Hancock, and G. Du. 2014. Temporal production of the signaling lipid phosphatidic acid by phospholipase D2 determines the output of extracellular signal-regulated kinase signaling in cancer cells. *Mol. Cell. Biol.* 34:84–95. https://doi.org/10.1128/MCB.00987-13

Downloaded from http://rupress.org/jcb/article-pdf/219/2/e201905190/1622245/jcb_201905190.pdf by guest on 05 December 2025